





A spatially restricted fibrotic niche in pulmonary fibrosis is sustained by M-CSF/M-CSFR signalling in monocyte-derived alveolar macrophages

Nikita Joshi^{1,7}, Satoshi Watanabe^{1,2,7}, Rohan Verma^{1,7}, Renea P. Jablonski^{1,3}, Ching-I Chen¹, Paul Cheresh^{1,4}, Nikolay S. Markov¹, Paul A. Reyfman ¹, Alexandra C. McQuattie-Pimentel¹, Lango Sichizya¹, Ziyang Lu¹, Raul Piseaux-Aillon¹, David Kirchenbuechler⁵, Annette S. Flozak¹, Cara J. Gottardi ¹, Carla M. Cuda⁶, Harris Perlman⁶, Manu Jain^{1,4}, David W. Kamp^{1,4}, G.R. Scott Budinger^{1,4,8} and Alexander V. Misharin^{1,8}

Affiliations: ¹Division of Pulmonary and Critical Care Medicine, Dept of Medicine, Feinberg School of Medicine, Northwestern University, Chicago, IL, USA. ²Dept of Respiratory Medicine, Kanazawa University Graduate School of Medical Sciences, Kanazawa, Japan. ³Dept of Medicine, Section of Pulmonary and Critical Care, The University of Chicago, Chicago, IL, USA. ⁴Dept of Medicine, Division of Pulmonary and Critical Care Medicine, Jesse Brown VA Medical Center, Chicago, IL, USA. ⁵Center for Advanced Microscopy, Robert H. Lurie Cancer Center, Feinberg School of Medicine, Northwestern University, Chicago, IL, USA. ⁶Division of Rheumatology, Dept of Medicine, Feinberg School of Medicine, Northwestern University, Chicago, IL, USA. ⁷These authors contributed equally to this work. ⁸These authors contributed equally to this work.

Correspondence: Alexander V. Misharin, Division of Pulmonary and Critical Care Medicine, Dept of Medicine, Feinberg School of Medicine, Northwestern University, Simpson Querrey Biomedical Research Center, 303 E. Superior Street, Chicago, IL 60611, USA. E-mail: a-misharin@northwestern.edu



@ERSpublications
Monocyte-derived alveolar macrophages orchestrate the development of the fibrotic niche, causally related to fibrosis and maintained via M-CSF/M-CSFR signalling <http://bit.ly/2nDjS20>

Cite this article as: Joshi N, Watanabe S, Verma R, *et al.* A spatially restricted fibrotic niche in pulmonary fibrosis is sustained by M-CSF/M-CSFR signalling in monocyte-derived alveolar macrophages. *Eur Respir J* 2020; 55: 1900646 [https://doi.org/10.1183/13993003.00646-2019].

ABSTRACT Ontologically distinct populations of macrophages differentially contribute to organ fibrosis through unknown mechanisms.

We applied lineage tracing, single-cell RNA sequencing and single-molecule fluorescence *in situ* hybridisation to a spatially restricted model of asbestos-induced pulmonary fibrosis.

We demonstrate that tissue-resident alveolar macrophages, tissue-resident peribronchial and perivascular interstitial macrophages, and monocyte-derived alveolar macrophages are present in the fibrotic niche. Deletion of monocyte-derived alveolar macrophages but not tissue-resident alveolar macrophages ameliorated asbestos-induced lung fibrosis. Monocyte-derived alveolar macrophages were specifically localised to fibrotic regions in the proximity of fibroblasts where they expressed molecules known to drive fibroblast proliferation, including platelet-derived growth factor subunit A. Using single-cell RNA sequencing and spatial transcriptomics in both humans and mice, we identified macrophage colony-stimulating factor receptor (M-CSFR) signalling as one of the novel druggable targets controlling self-maintenance and persistence of these pathogenic monocyte-derived alveolar macrophages. Pharmacological blockade of M-CSFR signalling led to the disappearance of monocyte-derived alveolar macrophages and ameliorated fibrosis.

Our findings suggest that inhibition of M-CSFR signalling during fibrosis disrupts an essential fibrotic niche that includes monocyte-derived alveolar macrophages and fibroblasts during asbestos-induced fibrosis.

Copyright ©ERS 2020. This article is open access and distributed under the terms of the Creative Commons Attribution Non-Commercial Licence 4.0.

Introduction

Pulmonary fibrosis is a complex process that is clinically characterised by a progressive increase in the number and size of spatially restricted areas of fibrosis [1]. Indeed, the three-dimensional distribution of these lesions on chest computed tomography combined with radiographic features of fibrotic regions is critical to the diagnosis and classification of pulmonary fibrosis. Single-cell RNA sequencing offers the opportunity to examine interactions between cell populations within these areas of fibrosis, but the process of tissue dissociation precludes understanding the spatial relationships between the cells [2]. We reasoned that a combination of genetic lineage tracing, single-cell RNA sequencing and single-molecule fluorescence *in situ* hybridisation could be combined with genetic or pharmacological interventions to identify conserved intracellular signalling events that might promote or sustain multicellular fibrotic niches in the lung. To test this hypothesis, we used a model of asbestos-induced lung fibrosis. Exposure to asbestos can induce the development of pulmonary fibrosis years after exposure has ceased [3], and historical and ongoing exposure to asbestos fibres remains an important occupational cause of pulmonary fibrosis. After inhalation, asbestos fibres remain lodged in small airways in rodents, creating spatially restricted regions of lung fibrosis [4–6].

Recently, investigators have identified several distinct macrophage populations in the lung. Tissue-resident alveolar macrophages originate from fetal monocytes, populate the alveolar niche soon after birth, are capable of self-renewal and, in mouse models, persist in the lung without appreciable input from myeloid cells over the lifespan of the animal [7–10]. Lung tissue-resident interstitial macrophages have been shown to include perivascular and peribronchial macrophages, which demonstrate distinct anatomical localisation and function [11–14]. In response to alveolar macrophage depletion and/or injury, monocytes are recruited to the lung where factors present in the microenvironment drive their differentiation into alveolar macrophages [15, 16]. Alveolar macrophages were recognised to play a critical role in asbestos-induced injury when DOSTERT *et al.* [17] reported that potassium currents in alveolar macrophages attempting to engulf asbestos fibres resulted in activation of the NLRP3 inflammasome, which is essential for the development of asbestos-mediated lung fibrosis [18]. Whether one or more of these macrophage populations is necessary for the development of fibrosis in response to asbestos remains unclear.

Here, we used a genetic lineage tracing system to show that tissue-resident alveolar macrophages and tissue-resident peribronchial and perivascular interstitial macrophages are present within the fibrotic niche, and that monocyte-derived alveolar macrophages do not originate from tissue-resident interstitial lung macrophages. Specific deletion of monocyte-derived alveolar macrophages reduced fibrosis severity. Single-molecule fluorescence *in situ* hybridisation demonstrated that monocyte-derived alveolar macrophages, expressing pro-fibrotic genes causally linked to fibrosis, were present within pathogenic multicellular niches that included injured epithelial cells and tissue fibroblasts. We then used single-cell transcriptomic analysis of lungs from mice treated with asbestos or bleomycin and patients with pulmonary fibrosis to look for intercellular interactions that sustain monocyte-derived alveolar macrophages. This analysis revealed macrophage colony-stimulating factor (M-CSF)/M-CSF receptor (M-CSFR) signalling as one of the key factors controlling monocyte-derived alveolar macrophages. Moreover, it provided unexpected evidence that expression of M-CSF in monocyte-derived alveolar macrophages could be involved in the maintenance of these cells in an autocrine manner. Interruption of M-CSF/M-CSFR signalling resulted in a selective loss of monocyte-derived alveolar macrophages within the fibrotic niche and an amelioration of lung fibrosis. These findings suggest that single-cell RNA sequencing data from multiple laboratories can be combined and validated to identify conserved intercellular interactions within multicellular fibrotic microdomains that might be targeted for the treatment of pulmonary fibrosis.

Materials and methods

Mice

All mouse procedures were approved by the Institutional Animal Care and Use Committee at Northwestern University (Chicago, IL, USA). All strains including wild-type mice were bred and housed at a barrier and specific pathogen-free facility at the Center for Comparative Medicine at Northwestern University. Mice aged 10–12 weeks were used for all experiments. C57BL/6J, *Cx3cr1^{ER-Cre}* mice [19] and *ZsGreen* [20] mice were obtained from Jackson Laboratories (Farmington, CT, USA). Floxed *Casp8^{fl/fl}*, *CD11c^{Cre}Casp8^{fl/fl}* and *CD11c^{Cre}Casp8^{fl/fl}Ripk3^{-/-}* mice have been described previously [9].

This article has supplementary material available from erj.ersjournals.com

Received: 1 April 2019 | Accepted after revision: 26 Sept 2019

Asbestos-induced lung fibrosis and drug administration

Mice aged 8–10 weeks were instilled intratracheally with control particles (TiO₂; 100 µg in 50 µL PBS) or crocidolite asbestos fibres (100 µg in 50 µL PBS) to induce lung fibrosis as described previously [21]. For lineage tracing studies, anaesthetised mice were administered tamoxifen by oral gavage (100 µL of 10 mg tamoxifen; Sigma, St Louis, MO, USA) dissolved in sterile corn oil (Sigma). Anti-CSF1 (M-CSF) antibody (0.5 mg, clone BE0204; BioXCell, West Lebanon, NH, USA) was administered intraperitoneally every 5 days and PLX3397 (40 mg·kg⁻¹; MedKoo Biosciences, Morrisville, NC, USA) was administered orally every day as described previously [22, 23]. Lungs were harvested at indicated time-points for flow cytometry, single-cell RNA sequencing, histopathology, immunohistochemistry and immunofluorescence.

Tissue preparation and flow cytometry

Tissue preparation for flow cytometry analysis and cell sorting was performed as described previously [9], with modifications. Briefly, mice were euthanised and their lungs were perfused through the right ventricle with 10 mL Hanks' balanced salt solution (HBSS). The lungs were removed and infiltrated with 2 mg·mL⁻¹ collagenase D (Roche, Indianapolis, IN, USA) and 0.2 mg·mL⁻¹ DNase I (Roche) dissolved in HBSS with Ca²⁺ and Mg²⁺, using a syringe with a 30G needle. Lungs were chopped with scissors, tissue was transferred into C-tubes (Miltenyi Biotech, Auburn, CA, USA) and processed in a GentleMACS dissociator (Miltenyi Biotech) using the m_lung_01 program, followed by incubation for 30 min at 37°C with gentle agitation, followed by the m_lung_02 program. The resulting single-cell suspension was filtered through a 40 µm nylon cell strainer mesh to obtain a single-cell suspension. The cells were incubated with anti-mouse CD45 microbeads (Miltenyi Biotech) and CD45⁺ cells were collected using a MultiMACS Cell24 Separator (Miltenyi Biotech) according to the manufacturer's protocol. Automated cell counting was performed (Cellometer K2; Nexcelom, Lawrence, MA, USA) with acridine orange/propidium iodide reagent. Cells were stained with fixable viability dye eFluor 506 (eBioscience, San Diego, CA, USA), incubated with FcBlock (BD Biosciences, San Jose, CA, USA) and stained with the following mixture of fluorochrome-conjugated antibodies (listed as antigen (clone, fluorochrome; manufacturer)): major histocompatibility complex II (2G9, BUV395; BD Biosciences), Ly6C (HK1.4, eFluor450; eBioscience), CD45 (30-F11, fluorescein isothiocyanate; eBioscience), CD64 (X54-5/7.1, phycoerythrin (PE); BioLegend, San Diego, CA, USA), Siglec F (E50-2440, PECF594; BD Biosciences), CD11c (HL3, PECy7; BD Biosciences), CD24 (M1/69, allophycocyanin; eBioscience), CD11b (M1/70, APCy7; BioLegend), Ly6G (1A8, Alexa 700; BD Biosciences) and NK1.1 (PK136, Alexa 700; BD Biosciences). Single-colour controls were prepared using BD CompBeads (BD Biosciences) and Arc beads (Invitrogen, Carlsbad, CA, USA). Flow cytometry was performed at the Northwestern University Robert H. Lurie Comprehensive Cancer Center Flow Cytometry Core Facility (Chicago, IL, USA). Data were acquired on a custom BD FACSymphony instrument using BD FACSDiva software (BD Biosciences). Compensation and analysis were performed using FlowJo software (TreeStar; www.flowjo.com). Each cell population was identified using a sequential gating strategy (supplementary figure S1a). The percentage of cells in the live/singlets gate was multiplied by the number of live cells using a Cellometer K2 image cytometer to obtain the cell count.

Single-cell RNA sequencing

Single-cell suspensions were prepared as described earlier with slight modification. Mice were euthanised with sodium pentobarbital overdose. The chest cavity was opened and lungs were perfused through the right ventricle with 10 mL HBSS. The lungs were removed and, using a 30G needle, infused with 1 mL dispase (Corning, Corning, NY, USA) with DNase I (Sigma) before incubation at room temperature with gentle agitation for 45 min, followed by gentle teasing using forceps into small (1–2 mm) fragments and incubation in digestion buffer for another 15 min. The resulting suspension was passed through a 70 µm cell strainer (Falcon; Corning), washed with DMEM (Corning) supplemented with 5% FBS (Corning), pelleted by centrifugation and erythrocytes were lysed using BD Pharm Lyse (BD Biosciences). The resulting single-cell suspension was kept in DMEM/FBS and passed through a 40 µm cell strainer (Falcon) two times. Cells were counted using a Cellometer K2 with nucleic acid binding dyes acridine orange to calculate total number of nucleated cells and propidium iodide to count dead cells; cell viability exceeded 85%. All manipulations were performed using wide-bore tips (Axygen; Corning). Single-cell 3' RNA sequencing libraries were prepared using Chromium Single Cell v2 Reagent Kit and Controller (10X Genomics, Pleasanton, CA, USA). Libraries were assessed for quality (TapeStation 4200; Agilent, Santa Clara, CA, USA) and then sequenced on an HiSeq 4000 instrument (Illumina, San Diego, CA, USA). Initial data processing was performed using the Cell Ranger version 2.0 pipeline (10X Genomics); reads were mapped to the mm10 version of the mouse genome. Analysis was performed using the Seurat R toolkit version 2.3.4 [24] for the dataset from Xi *et al.* [25] and version 3.0.2 [26] with scran normalisation [27] for the asbestos dataset. Analysis of the putative interactions between cells was performed using a curated list of ligands and receptors from the FANTOM5 project [28]. Analysis of RNA

velocity in single cells was performed using the velocity pipeline [29]. All code used for analysis can be found at <https://github.com/NUPulmonary/JoshiWatanabe2019>.

Data availability

Single-cell RNA sequencing data from TiO₂- and asbestos-exposed mice have been deposited with the Gene Expression Omnibus (GSE127803). We also used bulk RNA sequencing data on flow-sorted alveolar macrophages from GSE82158 [9], single-cell RNA sequencing data from patients with pulmonary fibrosis from GSE122960 [2] and mice exposed to bleomycin from GSE104154 [25]. Interactive plots from figures 4a, 4c and 7a are available for exploration at www.nupulmonary.org/resources.

Fluorescence in situ RNA hybridisation

Multiplex fluorescence *in situ* hybridisation was performed using RNAscope (Advanced Cell Diagnostics, Newark, CA, USA). Mouse lungs were inflated to 15 cmH₂O and fixed with 4% paraformaldehyde (EMS, Hatfield, PA, USA) for 24 h. Lungs were paraffin embedded and 5 µm tissue sections were mounted on Superfrost Plus slides (Thermo Fisher Scientific, Waltham, MA, USA). Slides were baked for 1 h at 60°C, deparaffinised in xylene and dehydrated in 100% ethanol. Sections were treated with H₂O₂ (Advanced Cell Diagnostics) for 10 min at room temperature and then heated to mild boil (98–102°C) in 1× target retrieval reagent buffer (Advanced Cell Diagnostics) for 15 min. Protease Plus (Advanced Cell Diagnostics) was applied to sections for 30 min at 40°C in a HyBEZ Oven (Advanced Cell Diagnostics). Hybridisation with target probes, pre-amplifier, amplifier, fluorescent labels and wash buffer (Advanced Cell Diagnostics) was done according to Advanced Cell Diagnostics' instructions for Multiplex Fluorescent Reagent Kit version 2 and 4-Plex Ancillary Kit version 2 when needed. Parallel sections were incubated with Advanced Cell Diagnostics positive and negative control probes. Sections were covered with ProLong Diamond Antifade Mountant (Invitrogen). Probes used were: mouse *Mrc1*, mouse *Pdgfa*, mouse *Pdgfra* and mouse *Csf1* (all Advanced Cell Diagnostics). Opal fluorophores (Opal 520, Opal 620 and Opal 690; Perkin Elmer, Shelton, CT, USA) were used at 1:1500 dilution in Multiplex TSA buffer (Advanced Cell Diagnostics). To validate colocalisation of *Mrc1* and either *Pdgfa* or *Csf1* probe, images were captured on a Nikon A1R confocal microscope (Tokyo, Japan) with ×20 and ×40 objectives, followed by uniform processing and pseudo-colouring in Fiji (<https://imagej.net/Fiji>). For quantification of *Mrc1* and *Pdgfa* co-staining, images of whole mouse lung tissue were captured on a Nikon Ti2 wide-field microscope with a ×20 objective and 0.45 NA. Quantification was performed using Nikon NIS-Elements software version 5.20.0 using the General Analysis module. Images were pre-processed with rolling ball background subtraction and segmented with thresholding. Objects positive for 4',6-diamidino-2-phenylindole (DAPI; Invitrogen) and *Mrc1*, DAPI and *Pdgfa*, and DAPI, *Mrc1* and *Pdgfa* were normalised to total number of cells.

Histopathology, immunohistochemistry and immunofluorescence

For histopathology and immunohistochemistry, mouse lung tissue from the regions adjacent to the regions used for flow cytometry and single-cell RNA sequencing was fixed in 4% paraformaldehyde for 24 h, dehydrated and embedded in paraffin; 4 µm thick sections were prepared. Haematoxylin/eosin staining and Masson's trichrome staining were performed for the analysis of fibrosis scoring. Immunohistochemistry was performed at the Northwestern University Mouse Histology and Phenotyping Laboratory Core Facility (Chicago, IL, USA).

For immunofluorescence, mouse lung tissue was fixed in 4% paraformaldehyde for 6 h and transferred into 20% sucrose for overnight incubation. Tissue was embedded in Tissue-Tek OCT compound (Sakura, Torrance, CA, USA), flash frozen in liquid nitrogen and cut on a cryostat at 14 µm thickness. Sections were air-dried and stained with PE-conjugated anti-proto-oncogene tyrosine-protein kinase MER (MERTK) (BioLegend), Alexa Fluor 647-conjugated anti-Siglec F (BD Biosciences), rabbit anti-resistin-like molecule-α (RELMα) (Abcam, Cambridge, MA, USA) and goat anti-surfactant protein C (SPC) (Santa Cruz Biotechnology, Dallas, TX, USA). Appropriate secondary antibodies were used for unconjugated primary antibody, including donkey anti-rabbit Alexa Fluor 647 (Invitrogen) and donkey anti-goat Alexa Fluor 568 (Invitrogen). DAPI was used for nuclear staining and sections were mounted with ProLong Diamond Antifade Mountant. Images were acquired on a Nikon A1R confocal microscope or Nikon Ti2 wide-field microscope at Northwestern University Nikon Cell Imaging Facility (Chicago, IL, USA), processed using Nikon Elements software.

Fibrosis scores and lung collagen determination

Fibrosis scores in mice were determined from haematoxylin/eosin- and Masson's trichrome-stained specimens in a blinded manner, in accordance with the code set by the Pathology Standards for Asbestosis as described previously [30]. Collagen levels were determined using the Sircol assay as described previously [21].

Statistical analysis

Statistical tests and tools for each analysis are explicitly described with the results or detailed in the figure legends.

Results

Recruitment of monocyte-derived alveolar macrophages distinguishes the response to asbestos from a nonfibrogenic particle (TiO₂)

We quantified monocyte and macrophage populations in the mouse lung *via* flow cytometry 14 days after intratracheal administration of asbestos, which reproducibly induces lung fibrosis, or a standard control particle TiO₂, which does not induce fibrosis (both 100 µg) (figure 1a; see supplementary figure S1a for gating strategy). We found that the numbers of monocytes and alveolar macrophages (CD64⁺Siglec F⁺) were similarly increased in mice administered either asbestos or TiO₂ when compared with naive mice (supplementary figure S1b). While the increase in alveolar macrophages was largely attributable to expansion of a Siglec F^{high} population in TiO₂-treated animals, the increase in alveolar macrophages in animals administered asbestos was attributable to both an expansion in Siglec F^{high} alveolar macrophages and the emergence of a population of Siglec F^{low} alveolar macrophages (~15% of the total alveolar macrophage pool) (figure 1b and c, and supplementary figure S1b).

We used a genetic lineage tracing system to determine whether Siglec F^{low} alveolar macrophages that were expanded in asbestos-treated animals but absent in TiO₂-treated animals were derived from the recruitment of monocytes or the expansion of tissue-resident alveolar macrophages. Circulating Ly6C^{high} classical monocytes express high levels of *Cx3cr1*, while tissue-resident alveolar macrophages do not [11, 19]. Accordingly, we crossed *Cx3cr1*^{ER-Cre} animals to ZsGreen reporter mice to track the fate of monocyte-derived cells in the lung during asbestos-mediated fibrosis (figure 1d). In this system, 7 days after tamoxifen administration 86.8% of circulating monocytes are green fluorescent protein (GFP)⁺ (figure 1e), but because they are short-lived, they disappear after tamoxifen pulse [19]. However, if GFP-labelled monocytes give rise to long-living macrophages, such as monocyte-derived alveolar macrophages, they will be permanently labelled with GFP, even after the expression of endogenous *Cx3cr1* has ceased. As expected, long-lived tissue-resident alveolar macrophages, which do not express *Cx3cr1*, were not labelled in this system (figure 1e). In contrast, 86.7% of the tissue-resident peribronchial and perivascular interstitial macrophages, which also express *Cx3cr1*, became GFP⁺ after tamoxifen pulse (figure 1e).

To assess the contribution of monocyte-derived macrophages to the expansion of the alveolar macrophage pool, reporter mice were treated with tamoxifen *via* oral gavage 7 and 8 days after administration of asbestos or TiO₂ and lungs were analysed by flow cytometry at day 14 (figure 1f). Administration of asbestos resulted in an influx of GFP⁺ alveolar macrophages, which were Siglec F^{low} and CD11b^{high} (figure 1g–i). In total, 4.9% of monocyte-derived alveolar macrophages (CD64⁺Siglec F^{low}) were GFP⁺ 1 week after tamoxifen pulse in asbestos-exposed mice (figure 1h and i). In contrast, in mice treated with TiO₂, only 1.4% of alveolar macrophages were GFP⁺, which was comparable to naive mice (figure 1h and i).

Monocyte-derived alveolar macrophages and not tissue-resident interstitial macrophages contribute to the macrophage pool in the fibrotic niche

We took advantage of the GFP label on monocyte-derived alveolar macrophages in our lineage tracing system to determine whether recruitment of these cells in response to asbestos was spatially restricted to areas near the fibres. Fibrosis was restricted to regions of bronchoalveolar duct junctions where asbestos fibres had lodged, but was absent in the distal lung (figure 2a). Immunofluorescent microscopy demonstrated that GFP⁺ cells were specifically found in these fibrotic areas, and both GFP⁺ and GFP⁻ cells appeared to engulf asbestos fibres (figure 2b and c). These cells are located in the alveolar space and express MERTK and Siglec F, confirming their identity as monocyte-derived alveolar macrophages (supplementary figure S2).

Tissue-resident interstitial macrophages (CD64⁺Siglec F⁻) have recently been reported to contribute to the population of tumour-associated macrophages [12]. To exclude the possibility that these tissue-resident peribronchial or perivascular interstitial macrophages can migrate to the alveolar space in response to asbestos-induced epithelial injury and differentiate into alveolar macrophages, we treated *Cx3cr1*^{ER-Cre} × ZsGreen reporter mice with tamoxifen to label tissue-resident interstitial macrophages (figure 2d). By 21 days after tamoxifen treatment, virtually all GFP-labelled monocytes disappeared from circulation, while 82% of tissue-resident interstitial macrophages remained GFP⁺ (figure 2d and e). These mice were treated with asbestos intratracheally and the lungs were analysed by flow cytometry 14 days later (figure 2d). The percentage of GFP⁺ alveolar macrophages in asbestos-exposed mice was not different

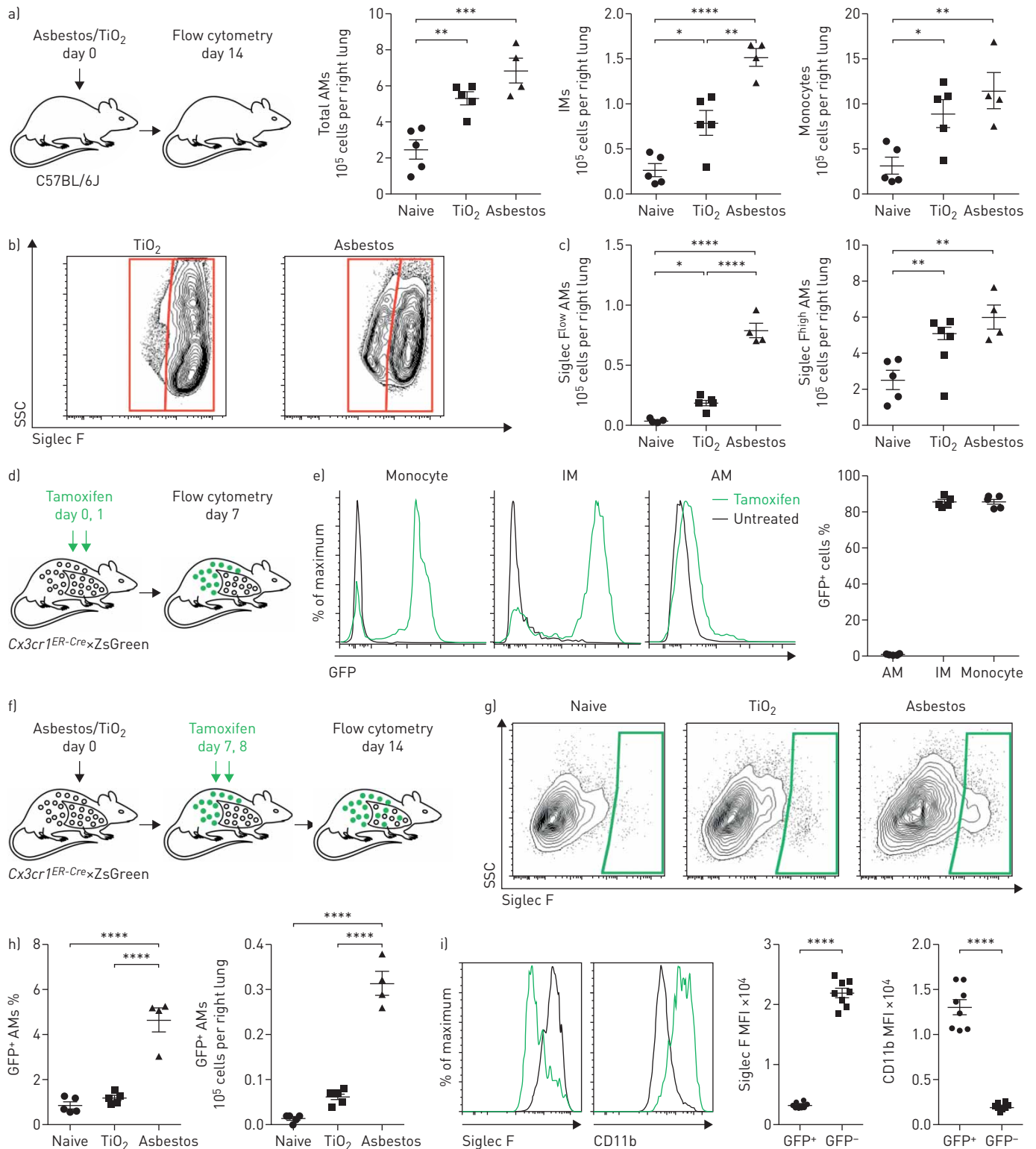


FIGURE 1 Exposure to asbestos or TiO₂ is distinguished by the recruitment of monocyte-derived alveolar macrophages (Mo-AMs) to the lung. IM: interstitial macrophage; SSC: side scatter; FSC: forward scatter; GFP: green fluorescent protein; MFI: median fluorescence intensity. a) Mice were administered crocidolite asbestos or TiO₂ (both at 100 μg intratracheally), and monocyte and macrophage populations were quantified by flow cytometry 14 days later [see supplementary figure S1a and b for gating strategy and quantification of other myeloid cell populations]. b) Representative contour plots gated on AMs (CD64⁺Siglec F⁺) from asbestos- or TiO₂-treated animals. c) Quantification of Siglec F^{low} and Siglec F^{high} AMs from naive, TiO₂- or asbestos-exposed animals according to gating in (b). d) Schematic of the experimental design for (e). e) *Cx3cr1*^{ER-Cre} × *ZsGreen* mice were treated with tamoxifen, and the percentage of GFP⁺ classical monocytes, IMs and AMs was assessed by flow cytometry. Representative histograms showing GFP expression are shown. f) Schematic of the experimental design for (g) and (h): lineage tracing system to track the ontogeny of AMs after intratracheal administration of asbestos or TiO₂. *Cx3cr1*^{ER-Cre} × *ZsGreen* mice were treated with asbestos

or TiO₂ and tamoxifen was administered as two boluses at days 7 and 8. The number of GFP⁺ AMs was analysed 7 days later. g) Representative contour plots and h) quantification of GFP⁺ Mo-AMs after asbestos or TiO₂ exposure. i) Representative histograms and MFI demonstrating expression of Siglec F and CD11b on Mo-AMs 14 days after exposure to asbestos. All data are presented as mean±SEM. n=4–5 mice per group. One-way ANOVA with the Tukey–Kramer test for multiple comparisons. *: p<0.05; **: p<0.01; ***: p<0.001; ****: p<0.0001. Representative data from two independent experiments.

from nonexposed mice, suggesting that monocytes, and not tissue-resident interstitial macrophages, drive the expansion of alveolar macrophages at the sites of asbestos-mediated injury and fibrosis (figure 2f).

Genetic deletion of monocyte-derived alveolar macrophages attenuates asbestos-induced pulmonary fibrosis

Previously, we have shown that a loss of caspase-8 in monocyte-derived alveolar macrophages results in their death *via* necroptosis during differentiation [9]. Accordingly, we used macrophage-specific deletion of *Casp8* with or without prevention of necroptosis through deletion of *Ripk3* to determine whether monocyte-derived alveolar macrophages are necessary for the development of asbestos-induced pulmonary fibrosis. Control mice (*Casp8*^{fl/fl}) and mice lacking caspase-8 in alveolar macrophages (*CD11c*^{Cre}*Casp8*^{fl/fl}) were administered either asbestos or TiO₂ intratracheally. The number of monocyte-derived alveolar macrophages (CD64⁺Siglec F^{low}) was significantly reduced in *CD11c*^{Cre}*Casp8*^{fl/fl} compared with *Casp8*^{fl/fl} controls 28 days after the administration of asbestos (figure 3a–d). Other cell populations were unchanged in *CD11c*^{Cre}*Casp8*^{fl/fl} mice compared with *Casp8*^{fl/fl} controls with the exception of eosinophils, which were reduced in *CD11c*^{Cre}*Casp8*^{fl/fl} mice compared with *Casp8*^{fl/fl} controls (figure 3e and supplementary figure S3a). *CD11c*^{Cre}*Casp8*^{fl/fl} mice showed less asbestos-induced fibrosis compared with *Casp8*^{fl/fl} controls (figure 3f–h). To confirm that the protection from fibrosis in *CD11c*^{Cre}*Casp8*^{fl/fl} mice resulted from necroptotic loss of monocyte-derived alveolar macrophages, we performed the same experiments in *CD11c*^{Cre}*Casp8*^{fl/fl}*Ripk3*^{-/-} mice and *Ripk3*^{-/-} mice. While the global loss of *Ripk3* did not affect the recruitment of monocyte-derived alveolar macrophages or the severity of fibrosis, the loss of *Ripk3* in *CD11c*^{Cre}*Casp8*^{fl/fl}*Ripk3*^{-/-} mice restored monocyte-derived alveolar macrophages and rescued asbestos-induced fibrosis (figure 3a–h). To determine whether tissue-resident alveolar macrophages also contributed to the development of asbestos-induced fibrosis, we depleted tissue-resident alveolar macrophages by treating mice with intratracheal liposomal clodronate 24 h prior to the administration of intratracheal asbestos or TiO₂. There was no difference in fibrosis 28 days later as determined by quantitative scoring of lung sections and measurements of lung soluble collagen using Picosirius red precipitation, suggesting that tissue-resident alveolar macrophages are not required for the development of fibrosis (supplementary figure S3b). These data demonstrate that monocyte-derived alveolar macrophages are necessary to develop a spatially restricted fibrotic niche in response to asbestos.

Single-cell RNA sequencing distinguishes responses to fibrogenic asbestos fibres and control particles

We reasoned that single-cell RNA sequencing combined with spatial techniques, such as *in situ* RNA hybridisation, could be used to gain insights into cellular interactions by which monocyte-derived alveolar macrophages are maintained and signal within fibrotic niches in the asbestos-exposed lung. Accordingly, we performed single-cell RNA sequencing on unenriched single-cell suspensions from the lungs of wild-type mice 14 days after exposure to either asbestos or TiO₂, when fibrosis is just beginning (one mouse per condition). Clustering was performed using the Seurat R toolkit and clusters were annotated based on the expression of cell-type-specific genes (figure 4a and supplementary table S1). After excluding doublets and low-quality cells, 15 288 cells from two libraries were used for subsequent analysis. We captured and resolved all major cell populations in the mouse lung, including interstitial and alveolar macrophages, alveolar epithelial type I and type II cells, dendritic cells, fibroblasts, mesothelial cells, smooth muscle cells, and subsets of endothelial cells. Each cluster included cells from both experimental groups (*i.e.* mice exposed to asbestos or TiO₂) (supplementary figure S4a and b). In agreement with our lineage tracing studies indicating influx of monocyte-derived alveolar macrophages, we identified a subcluster of alveolar macrophages (figure 4f) that was disproportionately represented by the cells from the asbestos-exposed animal (supplementary figure S4b).

We identified macrophages based on the expression of canonical macrophage-associated genes (*Cd68*, *Mrc1*, *Lyz2*, *Adgre1* and *Axl*) (figure 4b and supplementary figure S4c). Focused analysis of macrophage populations resolved two major populations identified as alveolar macrophages and tissue-resident interstitial macrophages. Tissue-resident interstitial macrophages could be further subdivided into peribronchial and perivascular macrophages, distinguished by expression of *Ccr2*, and *F13a1* and *Lyve1*, respectively (figure 4c–f and supplementary figure S4c) [11]. While some markers were expressed in both

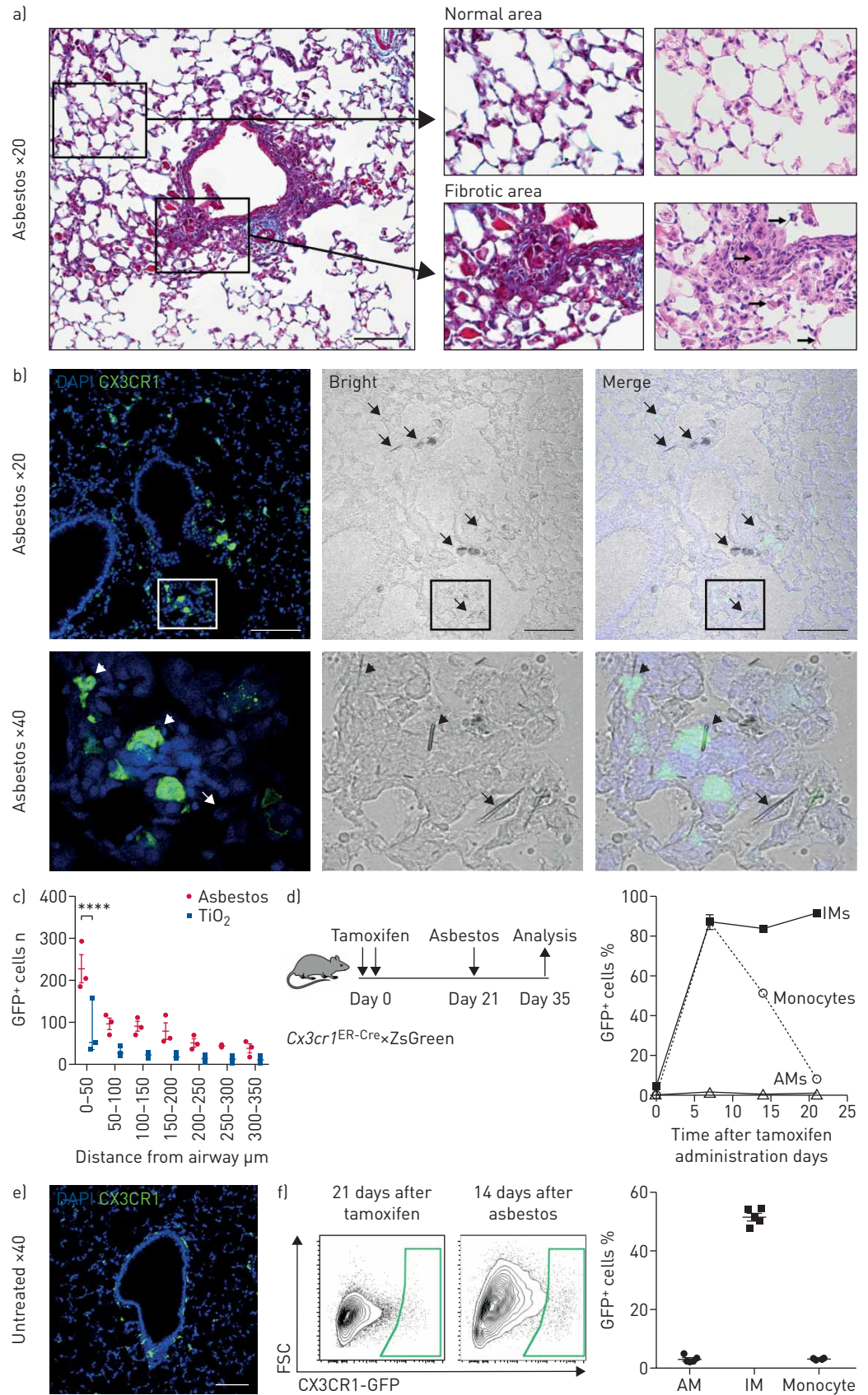


FIGURE 2 Recruitment of monocyte-derived alveolar macrophages (Mo-AMs) is spatially restricted to areas near asbestos fibres. DAPI: 4',6-diamidino-2-phenylindole; GFP: green fluorescent protein; IM: interstitial

macrophage; FSC: forward scatter. a) The intratracheal administration of asbestos fibres induces fibrosis near bronchoalveolar duct junctions where asbestos fibres lodge. Left panel: low-power image of a medium-sized airway (Mason's trichrome). Scale bar: 100 μ m. Right panels: high-power images (Mason's trichrome and haematoxylin/eosin, respectively). Areas of fibrosis develop adjacent to the airway in which asbestos fibres can be observed (arrows, bottom right panel). In contrast, alveolar structures in the distal lung parenchyma are relatively preserved. b) Top panels: representative lung histology from *Cx3cr1^{ER-Cre}* × *ZsGreen* mice treated with tamoxifen on day 14 and 15 (10 mg *via* oral gavage) and harvested 21 days after asbestos exposure. Scale bar: 100 μ m. Bottom row panels correspond to areas outlined in the boxes. Left panels: monocyte-derived cells are GFP⁺; nuclei stained with DAPI. Middle panels: phase contrast images; asbestos fibres are indicated by arrows. Right panels: merge. Bottom panels: asbestos fibres are surrounded by GFP⁺ cells (short arrows) and GFP⁻ cells (arrow) with macrophage morphology. c) Quantification of GFP⁺ Mo-AMs in peribronchial regions in asbestos- and TiO₂-treated mice. Two-way ANOVA with Tukey's multiple comparisons test. ****: $p < 0.0001$. d) Schematic of the experimental design, and kinetics of GFP⁺ monocytes, tissue-resident IMs and tissue-resident AMs after tamoxifen pulse in naive *Cx3cr1^{ER-Cre}* × *ZsGreen* mice. Percentage of GFP⁺ cells was assessed by flow cytometry. e) Representative fluorescent image showing GFP⁺ tissue-resident IMs 21 days after tamoxifen pulse in naive animals. f) Representative contour plots showing GFP expression gated on AMs from *Cx3cr1^{ER-Cre}* × *ZsGreen* mice 21 days after tamoxifen and 14 days after asbestos instillation. Percentage of GFP⁺ classical monocytes, IMs and AMs was assessed by flow cytometry. All data are presented as mean \pm SEM. $n = 3-5$ mice per group or time-point.

alveolar and interstitial macrophages (*Cd68*, *Mrc1*, *Lyz2*, *Adgre1* and *Axl*), others were restricted to alveolar macrophages (*Siglecf*, *Marco* and *Il18*) (supplementary figure S4c and supplementary table S2).

Alveolar macrophages contained three subclusters. Cluster AM1 was comprised of alveolar macrophages from mice exposed to either asbestos or TiO₂ (figure 4d and e). In contrast, clusters AM2 and AM3 were predominantly represented by cells from asbestos-exposed animals. Alveolar macrophages from cluster AM1 were characterised by expression of genes associated with normal homeostatic function of alveolar macrophages (*Ear1* and *Fabp1*) (supplementary figure S4d). Macrophages from cluster AM2 expressed genes involved in the inflammatory response, cytokine production and matrix metalloproteinase activation (*Car4*, *Ctsk*, *Chil3*, *S100a1* and *Wfdc21*) (supplementary figure S4d). In agreement with fate mapping studies, macrophages from cluster AM3 exhibited a more immature alveolar macrophage phenotype, characterised by lower expression of *Pparg*, *Car4*, *Ear1*, *Siglecf* and *Marco*, increased expression of *Itgam*, *Cd36* and *Gpnmb* (supplementary figure S4c and d), and increased expression of transcription factors involved in macrophage development and maintenance (*Litaf*, *Jund*, *Bhlhe40*, *Bhlhe41* and *Klf9*) and the unfolded protein response (*Atf3* and *Atf4*) (figure 4g). RNA velocity analysis [29] suggests that cluster AM3 represents a transcriptionally stable cell state, rather than an intermediate state between monocyte to tissue-resident macrophage differentiation (supplementary figure S4e and f).

We then queried the expression of 947 genes associated with pulmonary fibrosis using the Comparative Toxicogenomic Database [31] and found that 89 genes were detected in alveolar macrophages (figure 4h and supplementary figure S4g). Clusters AM1 and AM2 contained "generic" genes (21 and nine genes, correspondingly) associated with alveolar macrophage cellular identity and function (*Fabp1*, *Fabp4*, *Fabp5* and *Tgfb1*) [32]. In contrast, cluster AM3 was enriched for pro-fibrotic genes, and contained 59 genes involved in matrix remodelling and cell-cell interactions (*Cdh1*, *Fn1*, *Mmp12*, *Mmp14*, *Spp1* and *Timp2*) (figure 4h and supplementary figure S4g).

In a recent publication, Xie *et al.* [25] evaluated the response of fibroblasts in bleomycin-induced pulmonary fibrosis using single-cell RNA sequencing. While the authors focused their analysis on fibroblasts, their dataset contained a large number of nonmesenchymal cells, including alveolar macrophages (supplementary figure S4h and i, and supplementary table S3). Analysis of the macrophage population demonstrated the presence of three subclusters: AM1, AM2 and AM3 (supplementary figure S4j and supplementary table S4). Similar to our findings in asbestos, cluster AM1 was predominantly comprised of cells from PBS-treated control animals, while clusters AM2 and AM3 were comprised of cells from bleomycin-treated animals (supplementary figure S4k and l). Out of 947 genes associated with pulmonary fibrosis in the Comparative Toxicogenomic Database, we found 80 to be detected in alveolar macrophages from the bleomycin dataset (supplementary figure S4m). Cluster AM3 was enriched for expression of fibrosis-associated genes (53 genes), many of which overlapped with the AM3 cluster genes from our asbestos dataset (*Gpnmb*, *Fn1*, *Mmp12*, *Mmp14*, *Spp1* and *Timp2*) (supplementary figure S4g and m).

We have previously reported the emergence of a novel subpopulation of alveolar macrophages in lung explants from patients with pulmonary fibrosis compared with biopsies from normal donor lung [2]. 20 genes, including *SPP1*, *MMP14*, *TREM2* and *GNMB*, overlapped between the genes characterising the cluster of human pro-fibrotic alveolar macrophages from patients with pulmonary fibrosis and genes observed in the AM3 clusters from asbestos-induced and bleomycin-induced pulmonary fibrosis (supplementary figure S4n and supplementary table S5). Thus, our analysis has demonstrated the

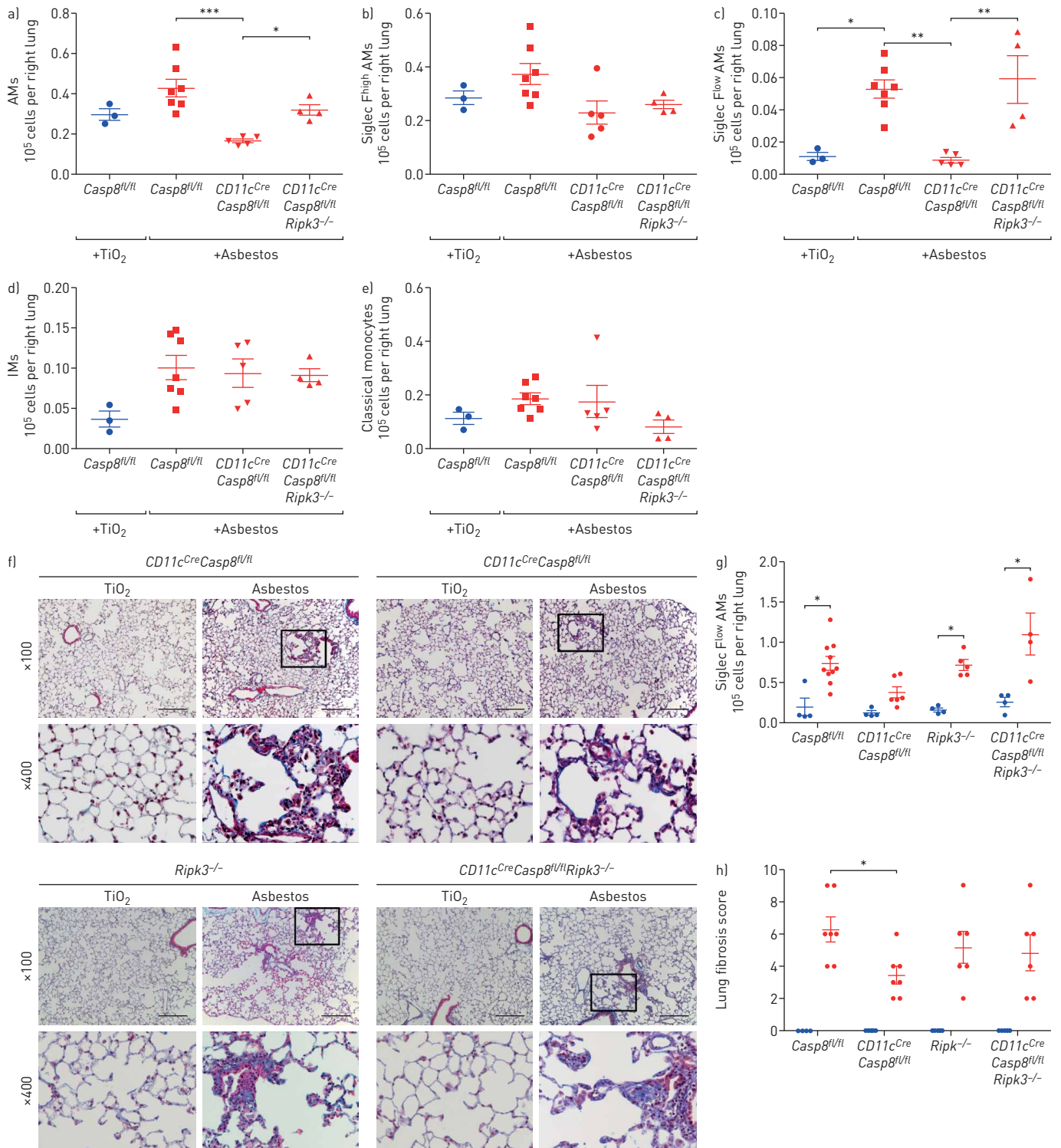


FIGURE 3 Deletion of monocyte-derived alveolar macrophages (AMs) attenuates asbestos-induced pulmonary fibrosis. IM: interstitial macrophage. *Casp8^{fl/fl}*, *CD11c^{Cre}Casp8^{fl/fl}*, *CD11c^{Cre}Casp8^{fl/fl}Ripk3^{-/-}* and *Ripk3^{-/-}* mice were administered crocidolite asbestos or TiO₂ (both at 100 µg intratracheally) and lungs were harvested 28 days later. a–e) Lungs were analysed using flow cytometry to quantify monocyte and macrophage populations. f) Representative histological images [Mason's trichrome]. Scale bar: 100 µm. g) Quantification of soluble collagen in lung homogenates. h) Lung fibrosis score: blinded scoring of a single longitudinal section from each mouse. Blue circles: TiO₂ treatment; red symbols: asbestos administration. All data are presented as mean ± SEM. n=3–7 mice per group. One-way ANOVA with the Tukey–Kramer test for multiple comparisons. *: p<0.05; **: p<0.01; ***: p<0.001.

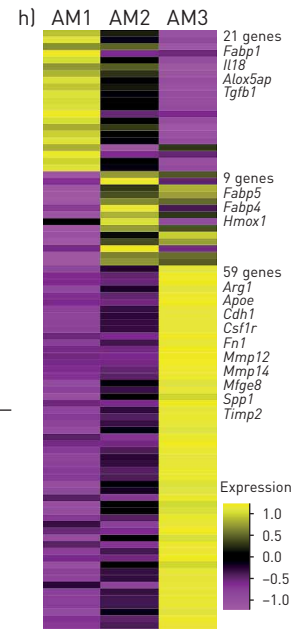
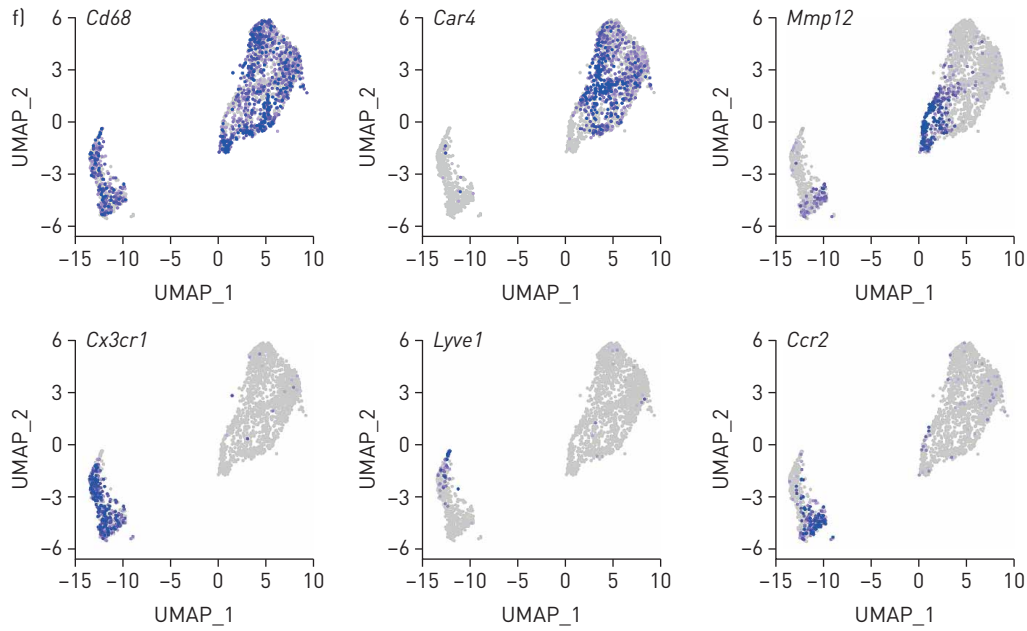
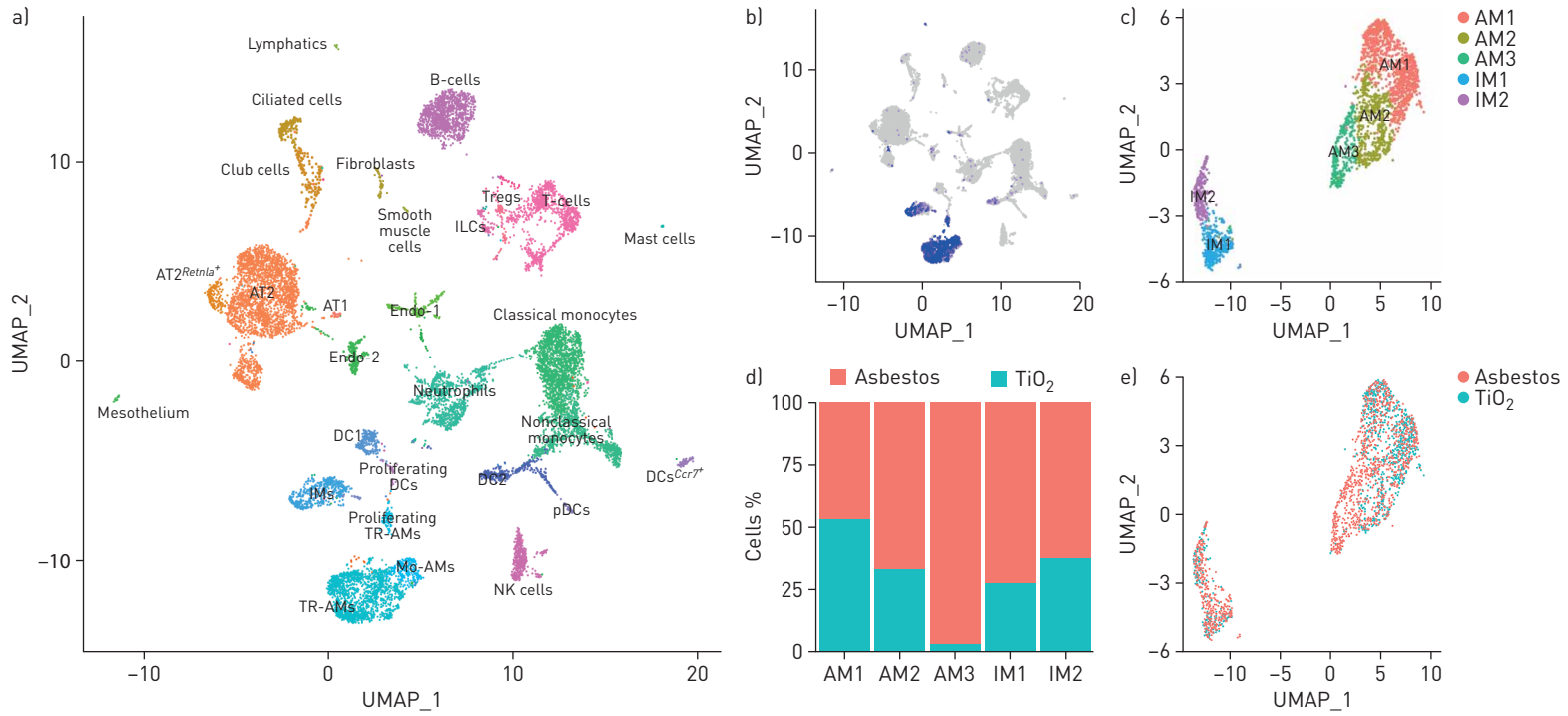


FIGURE 4 Single-cell RNA sequencing reveals pro-fibrotic monocyte-derived alveolar macrophages (Mo-AMs) during asbestos-induced pulmonary fibrosis. UMAP: uniform manifold approximation and projection; Treg: regulatory T-cell; AT1: alveolar epithelial type I cell; AT2: alveolar epithelial type II cell; Endo: endothelial cell; DC: dendritic cell; IM: interstitial macrophage; pDC: plasmacytoid DC; TR-AM: tissue-resident AM. a) UMAP plot demonstrating 26 cell clusters from 15452 cells identified by single-cell RNA sequencing 14 days after asbestos or TiO₂ exposure (one mouse per condition). b) Macrophages were identified using canonical lineage-restricted markers, such as *Mrc1*, as shown on the UMAP plot. c) Clusters of cells expressing *Mrc1* were subset from the main dataset and re-clustered, revealing two subclusters of tissue-resident lung IMs (IM1 and IM2) and three subclusters of AMs (AM1, AM2 and AM3). d) Bar plot and e) feature plot demonstrating the composition of macrophage subclusters in cells from asbestos- and TiO₂-exposed animals. f) Feature plots demonstrating expression of cluster-specific genes: *Cd68* as a pan-macrophage marker, *Car4* as a marker of mature TR-AMs (AM1 and AM2) and *Mmp12* as a marker of Mo-AMs (AM3). Tissue-resident IMs are characterised by expression of *Cx3cr1*, and can be further subdivided into perivascular [*Lyve1*] and peribronchial [*Ccr2*] IMs. g) Dot plot demonstrating the expression of transcription factors differentially expressed in Mo-AMs (AM3). h) Heatmap of 93 genes overlapping between AMs and pulmonary fibrosis-associated genes from the Comparative Toxicogenomic Database [947 genes as of February 2019]. Selected genes characterising clusters are shown; see supplementary figure S4e for the full list of genes. Interactive plots are available for exploration at www.nupulmonary.org/resources.

emergence of homologous populations in different models of pulmonary fibrosis (asbestos and bleomycin) and in patients with pulmonary fibrosis.

Single-cell RNA sequencing identifies ligand–receptor interactions that emerge during pulmonary fibrosis

Our data causally implicate monocyte-derived alveolar macrophages in the development of pulmonary fibrosis. To understand the molecular basis by which they signal to promote pulmonary fibrosis, we analysed possible ligand–receptor interactions that were identified in single-cell data from asbestos-treated lungs but were absent in TiO₂-treated lungs. Our initial analysis identified more than 50 000 possible interactions (supplementary figure S4o–q; see Data availability and online code for details) [28]. To narrow this list, we focused on the interactions between cell types located in physical proximity to areas of fibrosis (macrophages, fibroblasts and alveolar type II cells) and specifically focused on the two cell types that emerged exclusively during asbestos-induced pulmonary fibrosis: monocyte-derived alveolar macrophages and *Retnla*⁺ alveolar type II cells (supplementary figure S4r and supplementary table S6). We then went on to validate some of the identified interactions, specifically focusing on 1) factors that can promote recruitment of monocyte-derived alveolar macrophages by injured alveolar epithelial cells, 2) factors that can promote persistence of monocyte-derived alveolar macrophages in the fibrotic regions and 3) factors produced by monocyte-derived alveolar macrophages that can drive proliferation of fibroblasts.

M-CSF/M-CSFR signalling is necessary for the maintenance of monocyte-derived alveolar macrophages within fibrotic niches

Tissue-resident alveolar macrophages rely on granulocyte–macrophage colony-stimulating factor (GM-CSF; *Csf2*) produced by alveolar epithelial cells for their homeostatic maintenance [33]. In contrast, data from M-CSF-deficient mice and pharmacological blockade of M-CSFR (*Csf1r*) suggest that M-CSF (*Csf1*) signalling is dispensable for homeostatic maintenance of alveolar macrophages [34–36]. We found that *Csf1r* was upregulated in the AM3 cluster both in asbestos- and bleomycin-treated mice (figure 5a, and supplementary figure S4g and m). We asked which cells express *Csf1* and *Il34* (ligands for M-CSFR), and particularly whether any new *Csf1/Il34*-producing cells emerge during fibrosis. In TiO₂- and asbestos-exposed animals, *Il34* was expressed in alveolar type II cells and club cells, while *Csf1* was expressed in fibroblasts, mesothelium and endothelium (supplementary figure S5a and b). Interestingly, ~10% of macrophages in cluster AM3 expressed *Csf1* in both asbestos- and bleomycin-induced pulmonary fibrosis (figure 5a–c and supplementary table S6). Expression of *Csf1* was also detected by bulk RNA sequencing in flow-sorted macrophages from mice with bleomycin-induced fibrosis (from our previously published dataset [9]) (figure 5d). In humans, expression of *CSF1* was detected in alveolar macrophages from the lungs of normal donors and patients with pulmonary fibrosis (supplementary figure S5c), and expression of *CSF1R* was increased in patients with pulmonary fibrosis, specifically in the cluster containing pro-fibrotic alveolar macrophages (supplementary figure S5d and e). We then validated our findings using *in situ* RNA hybridisation. Double-positive *Mrc1*⁺*Csf1*⁺ alveolar macrophages were detected in the areas of fibrosis in proximity to *Pdgfra*⁺ fibroblasts 28 days after asbestos exposure (figure 5e and f, and supplementary figure S5f).

These data suggest that monocyte-derived alveolar macrophages are capable of generating an autocrine signal for their persistence. We tested this hypothesis using the *Cx3cr1*^{ER-Cre} × *ZsGreen* reporter mice described earlier. At 1 day prior to induction of pulmonary fibrosis *via* intratracheal administration of asbestos, we treated these mice with a pulse of tamoxifen to transiently label circulating monocytes and monocyte-derived alveolar macrophages derived from these monocytes (figure 5g). An established population of monocyte-derived alveolar macrophages was present in the lung 14 days after induction of

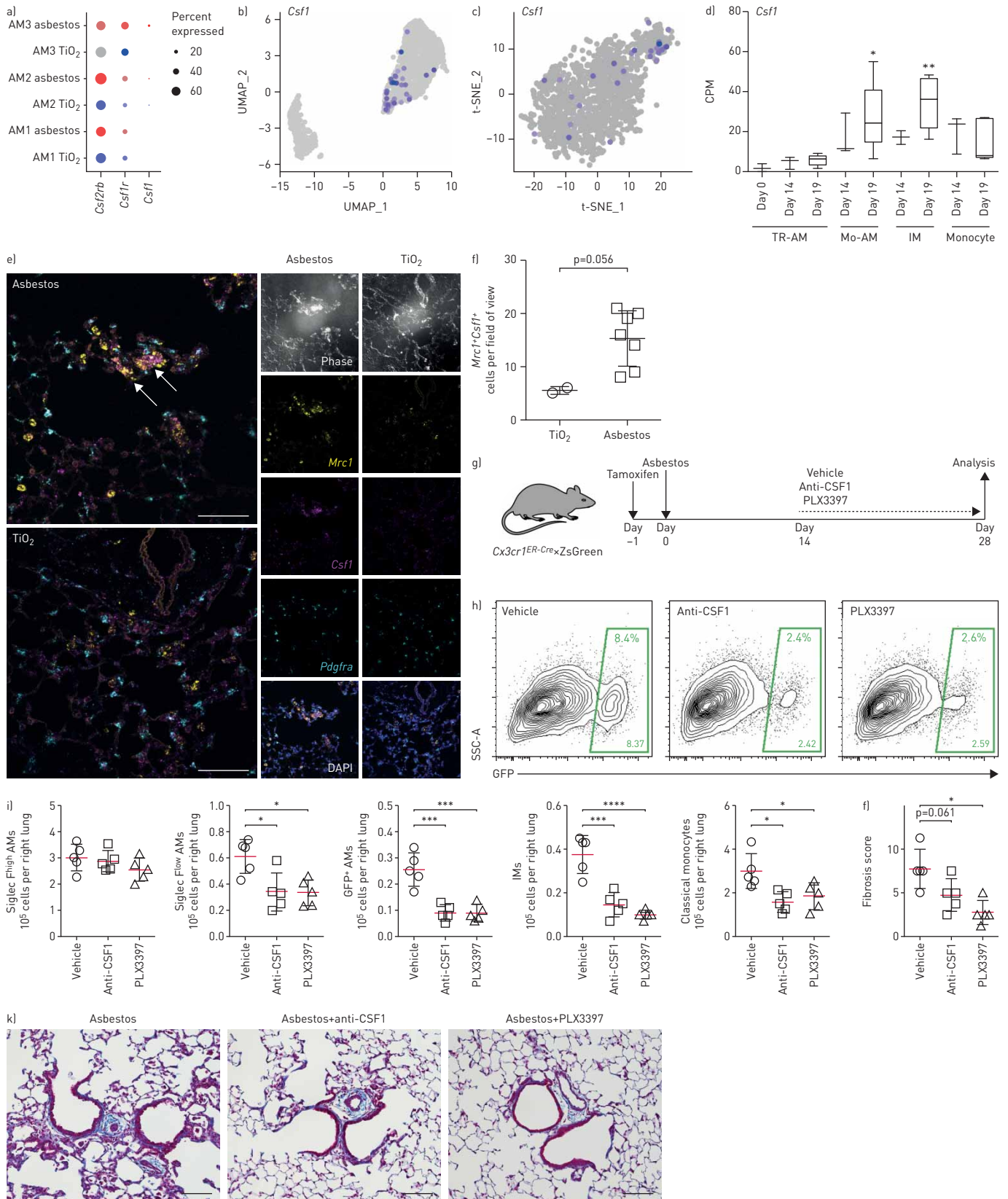


FIGURE 5 Autocrine macrophage colony-stimulating factor (M-CSF) signalling is required for maintenance of monocyte-derived alveolar macrophages (Mo-AMs) within fibrotic niches. UMAP: uniform manifold approximation and projection; t-SNE: t-distributed stochastic neighbour embedding; TR-AM: tissue-resident AM; IM: interstitial macrophage; SSC: side scatter; GFP: green fluorescent protein. a) Dot plot showing expression of *Csf2rb*, *Csf1r* and *Csf1* in subclusters of AMs after TiO_2 and asbestos exposure. b, c) Feature plots showing expression of *Csf1* in subcluster AM3 after b) asbestos and c) bleomycin exposure. d) Box and whisker plot shows expression of *Csf1* in flow-sorted AMs during the

course of bleomycin-induced pulmonary fibrosis [data from MISHARIN *et al.* [9]]. Box plot centre lines are median, box limits are upper and lower quartiles, and whiskers are minimal and maximal values. One-way ANOVA with Bonferroni correction for multiple comparisons. e) *In situ* RNA hybridisation confirms expression of *Csf1* in AMs during asbestos-induced pulmonary fibrosis. Analysis performed on day 28 after TiO₂ or asbestos exposure. Macrophages were identified as *Mrc1*⁺ cells and fibroblasts were identified as *Pdgfra*⁺ cells. Arrows indicate *Mrc1*⁺*Csf1*⁺ AMs. Scale bar: 50 µm. f) The number of *Mrc1*⁺*Csf1*⁺ AMs is increased after asbestos exposure. Data are from one mouse per condition. Mean±sd. Mann–Whitney test. g) Schematic of experimental design. *Cx3cr1*^{ER-Cre}×ZsGreen mice received a pulse of tamoxifen *via* oral gavage 1 day prior to administration of crocidolite asbestos (100 µg intratracheally). Starting at day 14 mice were treated with anti-CSF1 antibody (0.5 mg intraperitoneally, every 5 days) or PLX3397 (40 mg·kg⁻¹ orally, every day) and harvested at day 28. Numbers of monocytes and macrophages were measured by flow cytometry and the fibrosis score was analysed by histology at day 28. h) Representative flow cytometry plots gated on CD64⁺Siglec F⁺ AMs. i) Number of TR-AMs, Mo-AMs, IMs and classical monocytes from asbestos-exposed animals. j) Fibrosis score 28 days after asbestos exposure. k) Representative histological findings. Mason's trichrome. Scale bar 100 µm. Data are presented as mean±SEM. n=5 mice per group. One-way ANOVA with the Tukey–Kramer test for multiple comparisons. *: p<0.05; **: p<0.01; ***: p<0.001; ****: p<0.0001.

fibrosis (figure 1g and h). We then treated mice with neutralising anti-CSF1 antibody or with PLX3397 (a small molecule inhibitor of M-CSFR kinase signalling), and analysed pulmonary macrophage populations and pulmonary fibrosis severity 14 later (figure 5g). Pharmacological blockade of M-CSFR signalling decreased the number of monocyte-derived alveolar macrophages and decreased the severity of pulmonary fibrosis, while the number of tissue-resident alveolar macrophages was not affected and the level of circulating monocytes was only moderately reduced (figure 5h–k).

Monocyte-derived alveolar macrophages provide a link between epithelial injury and activation of resident fibroblasts within spatially restricted pro-fibrotic niches

Next, we queried both our asbestos and published bleomycin [25] alveolar macrophage single-cell RNA sequencing datasets for the expression of ligands that have partnering receptors on fibroblasts and could be involved in their proliferation. Using a curated database of ligand–receptor pairs [28], we identified that macrophages from the AM3 cluster in both asbestos- and bleomycin-treated mice expressed several molecules that could drive fibroblast proliferation, including *Pdgfa* (figure 6a and b, and supplementary table S6). We confirmed increased expression of *Pdgfa* in monocyte-derived alveolar macrophages by querying our bulk RNA sequencing data from flow-sorted macrophages from the bleomycin model (figure 6c) [9]. Furthermore, we validated our findings by performing *in situ* RNA hybridisation for *Mrc1*, *Pdgfa* and *Pdgfra* after asbestos exposure, and detected double-positive *Mrc1*⁺*Pdgfa*⁺ alveolar macrophages in the areas of fibrosis in proximity to *Pdgfra*⁺ fibroblasts (figure 6d and e, and supplementary figure S6).

Finally, to explore the possibility that monocyte-derived alveolar macrophages represent a link between asbestos-induced epithelial injury and fibroblast activation, we performed focused analysis of alveolar epithelial type II cells, which were well represented in our dataset. The analysis identified four subclusters. Subclusters AT2-1 and AT2-2 represented typical alveolar type II cells (figure 7a–c and supplementary figure S7). Subcluster AT2-3 contained cells from asbestos- and TiO₂-treated animals, and was characterised by the expression of *Krt8*, *Krt18*, *Ndnf* and *Lgals3* and matched recently described KRT8⁺ epithelial cells in the distal lung parenchyma (supplementary figure S7) [37]. Finally, cluster AT2-4 was comprised of cells found after asbestos exposure and expressed several genes linked to pulmonary fibrosis, including *Retnla* (RELMα), *Il33* and *Chia1* (supplementary figure S7d and supplementary table S7). *Retnla* is primarily expressed in epithelial cells and is thought to act as a chemoattractant for monocytes and monocyte-derived cells. Moreover, *Retnla*-deficient mice have been reported to be protected from experimental pulmonary fibrosis [38]. To see if the *Retnla*-expressing epithelial cells are restricted to areas of fibrosis, we treated *Cx3cr1*^{ER-Cre}×ZsGreen mice with tamoxifen 14 and 15 days after administration of asbestos or TiO₂ and analysed lungs using confocal immunofluorescent microscopy at day 21. Double-staining for RELMα and SPC confirmed that alveolar type II cells expressing RELMα were spatially restricted to areas of fibrosis, which also contained GFP⁺ monocyte-derived alveolar macrophages (figure 7e and f). Thus, our data suggest that monocyte-derived alveolar macrophages link spatially restricted epithelial injury and fibroblast proliferation.

Discussion

We performed an integrated analysis of single-cell RNA sequencing data from lung tissue of patients with pulmonary fibrosis and two murine models of lung fibrosis to identify putative mechanisms of intracellular communication within the fibrotic niche. From this analysis, we predicted that monocyte-derived alveolar macrophages drive fibrosis and are capable of self-maintenance *via* autocrine M-CSF/M-CSFR signalling. We used a genetic lineage tracing system and single-molecule *in situ* RNA hybridisation to show that *Csf1*- and *Pdgfa*-expressing monocyte-derived alveolar macrophages, *Retnla*-expressing epithelial cells, and *Pdgfra*-expressing fibroblasts are localised to fibrotic niches within the lung near asbestos fibres. We then used genetic and pharmacological strategies to causally link *Csf1*-expressing monocyte-derived alveolar macrophages to fibrosis. These findings demonstrate the power of a combined approach using single-cell

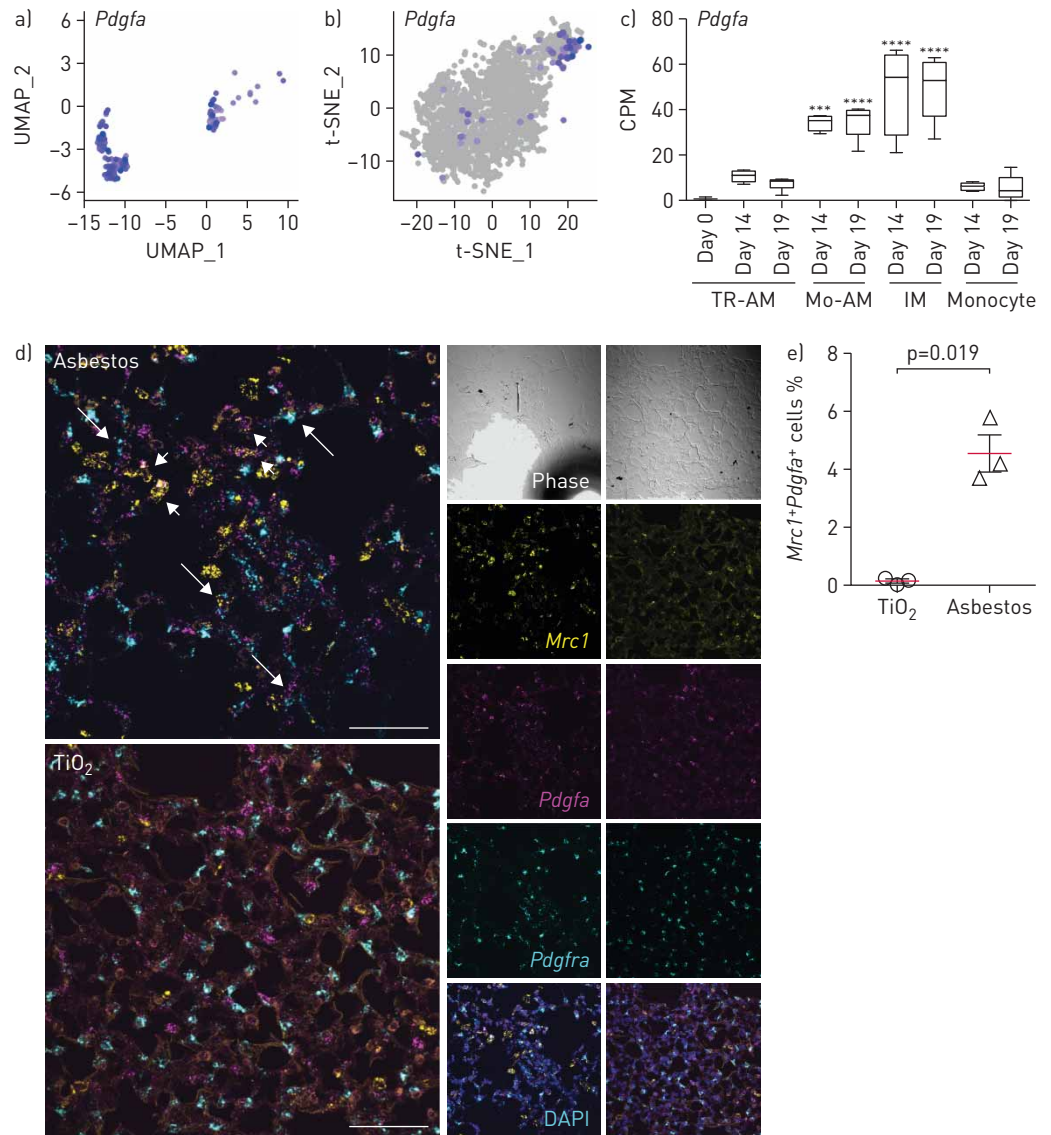


FIGURE 6 Monocyte-derived alveolar macrophages [Mo-AMs] express *Pdgfa* which is required for fibroblast proliferation. UMAP: uniform manifold approximation and projection; t-SNE: t-distributed stochastic neighbour embedding; TR-AM: tissue-resident AM; IM: interstitial macrophage. a, b) UMAP and t-SNE plots showing expression of *Pdgfa* in AMs after a) asbestos and b) bleomycin exposure. c) Bar plot showing expression of *Pdgfa* in flow-sorted AMs during the course of bleomycin-induced pulmonary fibrosis. Data from MISHARIN *et al.* [9]. Box plot centre lines are median, box limits are upper and lower quartiles, and whiskers are minimal and maximal values. One-way ANOVA with Bonferroni correction for multiple comparisons. ***: $p < 0.001$; ****: $p < 0.0001$. d) *In situ* RNA hybridisation confirms expression of *Pdgfa* in AMs during pulmonary fibrosis. Analysis performed on day 28 after TiO₂ or asbestos exposure. Macrophages were identified as *Mrc1*⁺ cells and fibroblasts were identified as *Pdgfra*⁺ cells. Short arrows indicate *Mrc1*⁺*Pdgfa*⁺ macrophages and long arrows indicate *Pdgfra*⁺ fibroblasts adjacent to *Mrc1*⁺*Pdgfa*⁺ macrophages. Scale bar: 50 μ m. e) The percentage of *Mrc1*⁺*Pdgfa*⁺ AMs is increased after asbestos exposure. Data are from three mice per condition. Mean \pm SD. Mann-Whitney test.

RNA sequencing from humans and mice, spatial transcriptomics, genetic lineage tracing, and causal interventions in mouse models to unravel the complex intercellular interactions necessary for fibrosis.

Single-cell RNA sequencing is transforming our understanding of biology by revealing heterogeneity within cell populations that emerge during disease. We show that single-cell RNA sequencing can be used to combine data generated by different laboratories in different animal models of disease with homologous data from diseased patients to identify common mechanisms in disease pathogenesis [2, 25]. By using a genetic lineage tracing system that marks the ontogeny of recruited macrophages, we were able to spatially localise intercellular signals predicted from single-cell RNA sequencing data to areas of fibrosis surrounding asbestos

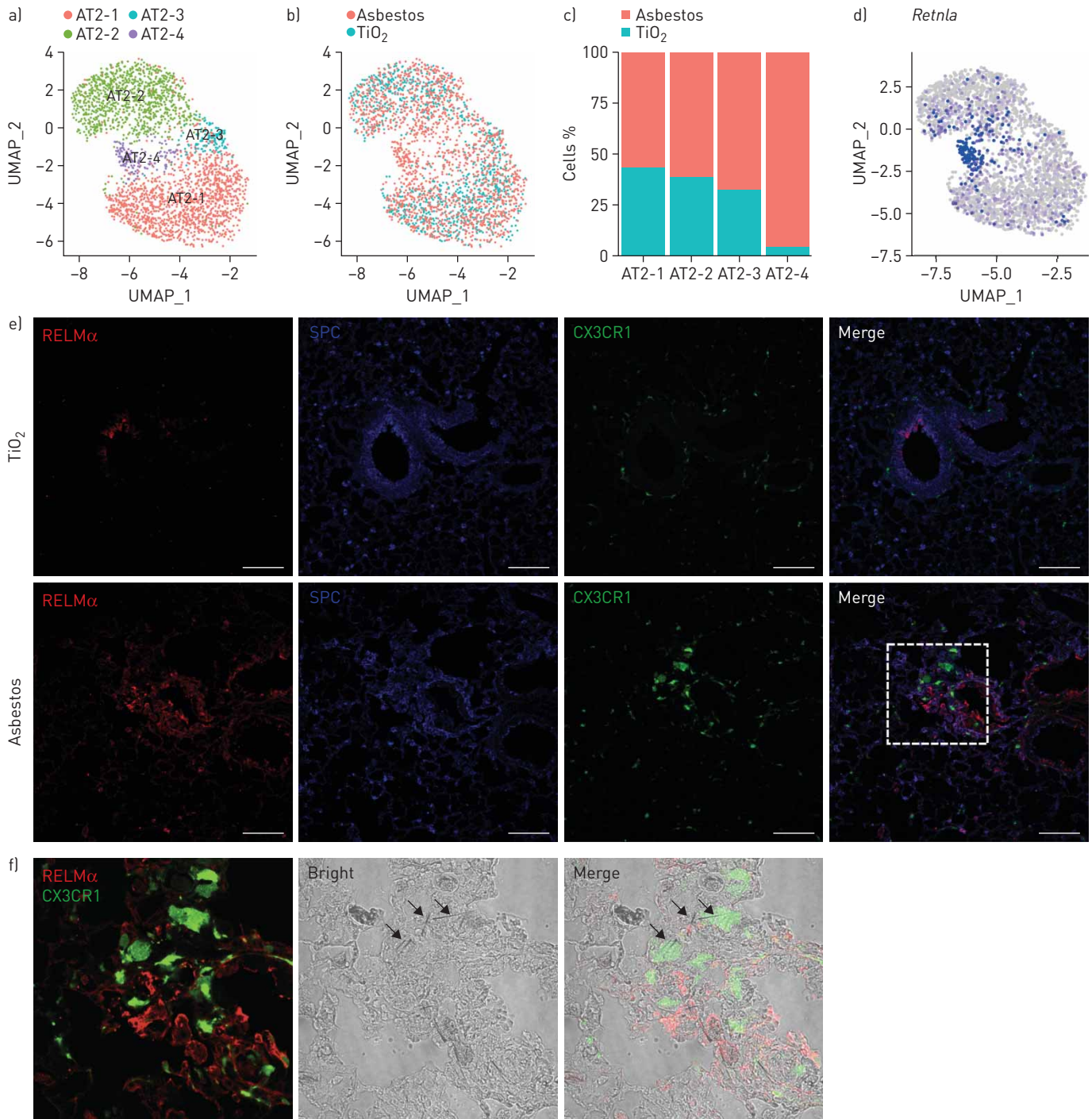


FIGURE 7 Expression of resistin-like molecule- α (RELMA) is restricted to epithelial cells located in the areas of fibrosis. UMAP: uniform manifold approximation and projection; SPC: surfactant protein C. a) UMAP plot demonstrating subclusters of alveolar type II cells. b) UMAP plot and c) bar plot demonstrating composition of the alveolar type II cell subclusters. d) Feature plot demonstrating increased expression of *Retnla* in alveolar type II cells 14 days after asbestos exposure. e) *Cx3cr1*^{ER-Cre} \times ZsGreen mice were administered with asbestos intratracheally and treated with tamoxifen at days 14 and 15 after exposure; lungs were harvested for analysis at day 21. Representative fluorescent images showing expression of RELMA (red), SPC (blue) and CX3CR1-green fluorescent protein (green) in lungs from TiO₂- or asbestos-treated animals at day 21 post-exposure. RELMA is detected in the airway epithelial cells and alveolar type II cells in the fibrotic regions in the asbestos model, but not in alveolar type II cells after TiO₂ exposure. Scale bar: 100 μ m. f) Enlargement of the box in (e): RELMA-positive epithelial cells (red) and monocyte-derived alveolar macrophages (green) are co-localised with asbestos fibres. Experimental design same as in (e).

fibres in the mouse lung. Computational consolidation of single-cell RNA sequencing datasets generated in other models of fibrosis is a promising approach to generate hypotheses with respect to fibrosis pathogenesis that can be tested with causal genetic or pharmacological interventions [39].

Our findings suggest the emergence of spatially restricted multicellular pro-fibrotic niches during pulmonary fibrosis. In these niches, injured epithelial cells drive recruitment of monocyte-derived alveolar macrophages, which, in turn, provide signals for fibroblast proliferation. Tissue-resident macrophages outside the lung rely on growth factors produced by other cells comprising the niche [40], particularly on M-CSF produced by fibroblasts [41]. In contrast, tissue-resident alveolar macrophages in the lung do not require M-CSF but do require GM-CSF for their maintenance, which is normally produced by alveolar type II cells [8, 33]. We found that monocyte-derived alveolar macrophages in mouse models of pulmonary fibrosis and (possibly monocyte-derived) pro-fibrotic alveolar macrophages in patients with pulmonary fibrosis were characterised by increased expression of *Csf1r/CSF1R*. Similar upregulation of *CSF1R* expression on fibrosis-associated macrophages can be found in the recent independent single-cell transcriptomic analysis of the lungs from patients with idiopathic pulmonary fibrosis, indicating high reproducibility of our findings [42]. Detection of *Csf1/CSF1* expression in these alveolar macrophages suggests they can maintain their population in the fibrotic niche *via* autocrine production of M-CSF, thus becoming independent of signals from other resident lung cells for their survival as was recently postulated in an elegant computational model of fibrosis containing macrophages and fibroblasts [41, 43]. We confirmed this hypothesis by showing two pharmacological strategies to inhibit CSF1 signalling reduced the number of monocyte-derived alveolar macrophages in the niche and reduced the severity of asbestos-induced fibrosis. Autocrine M-CSF signalling may provide a mechanism by which macrophages are sustained at the “advancing front” of fibroblastic foci where normal signals from the alveolar epithelium and mesenchyme are lacking [44]. In this niche, pro-fibrotic macrophages secrete factors essential for fibroblast proliferation, including platelet-derived growth factor subunit A (PDGFA), which was also elevated in alveolar macrophages from patients with pulmonary fibrosis [45, 46]. Our results and those from another group studying radiation-induced lung fibrosis support therapeutic consideration of M-CSF/M-CSFR inhibition for the treatment of some forms of pulmonary fibrosis [47]. It is of interest that monocyte-derived alveolar macrophages recruited to the lung during bleomycin also express M-CSF and M-CSFR, but bleomycin-induced fibrosis resolves spontaneously. Combining our lineage tracing system with single-cell RNA sequencing data from resolving bleomycin-induced fibrosis and persistent asbestos-induced fibrosis might suggest how monocyte-derived alveolar macrophages change as fibrosis resolves.

Using previously validated genes as markers, we resolved three previously described transcriptionally and anatomically distinct populations of macrophages in the normal murine lung from single-cell RNA sequencing data: alveolar macrophages, peribronchial interstitial macrophages and perivascular interstitial macrophages [11, 13]. We used a genetic lineage tracing system to distinguish between tissue-resident interstitial macrophages, tissue-resident alveolar macrophages and monocyte-derived alveolar macrophages that we predicted would emerge during asbestos-induced fibrosis based on work from our group that has been confirmed by others [9, 48, 49]. All three populations were present within the fibrotic niche, but only monocyte-derived alveolar macrophages were uniquely found in areas of fibrosis. Lineage tracing studies showed these monocyte-derived alveolar macrophages do not arise from interstitial macrophages. Tissue-resident interstitial macrophages did not expand, become activated or differentiate into alveolar macrophages during fibrosis and depletion of monocyte-derived but not tissue-resident alveolar macrophages ameliorated fibrosis severity. We combined our single-cell RNA sequencing data of asbestos-induced fibrosis with a recently published single-cell RNA sequencing dataset from bleomycin-induced fibrosis [25] to demonstrate the existence of the homologous macrophage populations in both models. Moreover, we show that during the later stages of fibrosis monocyte-derived alveolar macrophages represent a transcriptionally homogenous population during fibrosis. In contrast, high-resolution profiling of the early stages of bleomycin-induced pulmonary fibrosis across multiple time-points demonstrated heterogeneity of monocyte-derived macrophages [37]. These effects are likely a combination of cell autonomous changes related to monocyte to macrophage differentiation and environmentally driven transcriptional programs related to the spatial localisation of monocyte-derived alveolar macrophages to areas of injury as we report here, and as we found in bleomycin-induced fibrosis using a distinct lineage tracing system [10].

We have previously shown that macrophage-specific deletion of *Casp8* results in the death of monocytes as they differentiate into alveolar macrophages *via* necroptosis as evidenced by a rescue of fibrosis severity when *Casp8* and *Ripk3* are simultaneously deleted [9]. We took advantage of this system to genetically demonstrate a causal role for monocyte-derived alveolar macrophages in the development of asbestos-induced lung fibrosis. In contrast, deletion of tissue-resident alveolar macrophages through the administration of intratracheal liposomal clodronate prior to asbestos exposure had no effect on fibrosis severity. These findings suggest caution in interpreting the results of “alveolar macrophage-specific deletion” of genes during fibrosis. Monocyte to alveolar macrophage differentiation involves reshaping of >70% of the cellular transcriptome and requires multiple transcriptional pathways. Deletion of any gene necessary for monocyte to alveolar macrophage differentiation might therefore reduce or eliminate

monocyte-derived alveolar macrophages and ameliorate fibrosis. These effects might be independent of the described function of the gene in mature alveolar macrophages [15]. For example, monocyte/alveolar macrophage deletion of *Tgfb1* [50], *Torc1* [51], *Pparg* [52], *Casp8* [9] or *Cflar* [48] will prevent monocyte to macrophage differentiation, which likely in part explains their salutary effects on fibrosis or airway inflammation.

Our study has limitations. First, while we used a validated lineage tracing system to exclude the possibility that tissue-resident peribronchial or perivascular interstitial macrophages serve as a significant source of pro-fibrotic alveolar macrophages, it is possible that they regulate the recruitment or differentiation of monocytes in response to pro-fibrotic stimulus as has been recently described [14]. Second, while our single-cell RNA sequencing analysis was able to capture and resolve many of the canonical cell types identified in the mouse lung, several cell types, including alveolar type I cells, fibroblasts and smooth muscle cells/myofibroblasts, were under-represented in our dataset. Thus, we were not able to resolve heterogeneity within these populations during pulmonary fibrosis. Other techniques, such as enrichment for specific populations of interest or single-nucleus RNA sequencing, may address these limitations [25, 53, 54].

In summary, we found that recruitment of monocyte-derived alveolar macrophages is limited to spatially restricted fibrotic niches in pulmonary fibrosis. Genes expressed by injured epithelial cells, monocyte-derived macrophages and fibroblasts can be detected using single-cell RNA sequencing and then used to guide spatial assays (such as *in situ* RNA hybridisation) to reconstruct multicellular niches necessary for the development and maintenance of fibrosis. Genetically inducing deletion of monocyte-derived alveolar macrophages by necroptosis during their differentiation ameliorated lung fibrosis, causally linking them to disease pathogenesis. Single-cell RNA sequencing suggested monocyte-derived alveolar macrophages sustain themselves through M-CSF/M-CSFR signalling and the administration of antibodies to M-CSF or blockade of M-CSFR with small molecule inhibitors resulted in a loss of already established populations of monocyte-derived alveolar macrophages. While other populations, such as activated fibroblasts, could act as a source of M-CSF to sustain the population of monocyte-derived alveolar macrophages, single-cell RNA sequencing and fluorescence *in situ* RNA hybridisation data suggest that monocyte-derived alveolar macrophages express *Csf1*, raising an intriguing possibility that these cells can maintain their population *via* an autocrine M-CSF/M-CSFR loop. If true, this finding could be of high importance, suggesting that pathogenic monocyte-derived alveolar macrophages can sustain their population and drive fibroblast proliferation even in the absence of active epithelial injury [43]. Collectively, our results support the combination of lineage tracing, computational integration of single-cell RNA sequencing datasets from murine and human fibrosis, and *in situ* RNA hybridisation imaging as a powerful method to identify pathways that can be targeted for the treatment of different disease endotypes in patients with pulmonary fibrosis.

Acknowledgements: This work was supported by the Office of the Assistant Secretary of Defense for Health Affairs, through the Peer Reviewed Medical Research Program under Award W81XWH-15-1-0215 to G.R.S. Budinger and A.V. Misharin. Opinions, interpretations, conclusions and recommendations are those of the authors and are not necessarily endorsed by the Dept of Defense. Next-generation sequencing on the Illumina HiSeq 4000 was performed by the NUSeq Core Facility, which is supported by the Northwestern University Center for Genetic Medicine, Feinberg School of Medicine, and Shared and Core Facilities of the University's Office for Research. Northwestern University Flow Cytometry Facility, Center for Advanced Microscopy and Pathology Core Facility are supported by NCI Cancer Center Support Grant P30 CA060553 awarded to the Robert H. Lurie Comprehensive Cancer Center. Multiphoton microscopy was performed on a Nikon A1R multiphoton microscope, acquired through the support of NIH 1S10OD010398-01. This research was supported in part through the computational resources and staff contributions provided by the Genomics Computing Cluster (Genomic Nodes on Quest), which is jointly supported by the Feinberg School of Medicine, the Center for Genetic Medicine, and Feinberg's Dept of Biochemistry and Molecular Genetics, the Office of the Provost, the Office for Research, and Northwestern Information Technology.

Author contributions: N. Joshi: designed the study, performed experiments, analysed results, performed bioinformatics analysis, wrote the manuscript. S. Watanabe: designed the study, performed experiments, analysed results, wrote the manuscript. R. Verma: performed bioinformatics analysis, wrote the manuscript. R.P. Jablonski, C-I Chen, P. Cheresch: performed experiments, analysed results. P.A. Reyfman, N.S. Markov: performed bioinformatics analysis. A.C. McQuattie-Pimentel, Z. Lu, L. Sichizya, R. Piseaux-Aillon, A.S. Flozak: performed experiments, analysed results. D. Kirchenbuechler: performed analysis of the RNAscope experiments. C.J. Gottardi: analysed results, wrote the manuscript. C.M. Cuda, H. Perlman: developed and provided genetically modified animals, provided reagents and resources. M. Jain: provided reagents and resources, wrote the manuscript. D.W. Kamp: designed and supervised the study, provided reagents and resources, wrote the manuscript. G.R.S. Budinger and A.V. Misharin: designed and supervised the study, performed analysis, wrote the manuscript, provided funding for the project. All authors discussed the results and commented on the manuscript.

Conflict of interest: None declared.

Support statement: S. Watanabe is supported by MSD Life Science Foundation, Public Interest Incorporated Foundation, Japan, and David W. Cugell and Christina Enroth-Cugell Fellowship Program at Northwestern University. P.A. Reyfman

is supported by Northwestern University's Lung Sciences Training Program 5T32HL076139-13 and 1F32HL136111-01A1. H. Perlman is supported by NIH grants AR064546, HL134375, AG049665 and UH2AR067687; and the United States–Israel Binational Science Foundation (2013247), the Rheumatology Research Foundation (Agmt 05/06/14), Mabel Greene Myers Professor of Medicine and generous donations to the Rheumatology Precision Medicine Fund. C.J. Gottardi is supported by NIH grant HL143800. M. Jain is supported by Veterans Administration grant BX000201. D.W. Kamp is supported by Veterans Affairs Merit Award 2IO1BX000786-05A2. G.R.S. Budinger is supported by NIH grants ES013995, HL071643 and AG049665, Veterans Administration grant BX000201 and Dept of Defense grant PR141319. A.V. Misharin is supported by NIH grants HL135124, AG049665 and AII35964 and US Dept of Defense grant PR141319. Funding information for this article has been deposited with the Crossref Funder Registry.

Conflict of interest: N. Joshi has nothing to disclose.

References

- Raghu G, Remy-Jardin M, Myers JL, *et al.* Diagnosis of idiopathic pulmonary fibrosis. An official ATS/ERS/JRS/ALAT clinical practice guideline. *Am J Respir Crit Care Med* 2018; 198: e44–e68.
- Reyfman PA, Walter JM, Joshi N, *et al.* Single-cell transcriptomic analysis of human lung provides insights into the pathobiology of pulmonary fibrosis. *Am J Respir Crit Care Med* 2019; 199: 1517–1536.
- Cugell DW, Kamp DW. Asbestos and the pleura: a review. *Chest* 2004; 125: 1103–1117.
- Adamson IY, Bowden DH. Response of mouse lung to crocidolite asbestos. 2. Pulmonary fibrosis after long fibres. *J Pathol* 1987; 152: 109–117.
- Adamson IY, Bowden DH. Response of mouse lung to crocidolite asbestos. 1. Minimal fibrotic reaction to short fibres. *J Pathol* 1987; 152: 99–107.
- Roggli VL, George MH, Brody AR. Clearance and dimensional changes of crocidolite asbestos fibers isolated from lungs of rats following short-term exposure. *Environ Res* 1987; 42: 94–105.
- Janssen WJ, Barthel L, Muldrow A, *et al.* Fas determines differential fates of resident and recruited macrophages during resolution of acute lung injury. *Am J Respir Crit Care Med* 2011; 184: 547–560.
- Guilliams M, De Kleer I, Henri S, *et al.* Alveolar macrophages develop from fetal monocytes that differentiate into long-lived cells in the first week of life via GM-CSF. *J Exp Med* 2013; 210: 1977–1992.
- Misharin AV, Morales-Nebreda L, Reyfman PA, *et al.* Monocyte-derived alveolar macrophages drive lung fibrosis and persist in the lung over the life span. *J Exp Med* 2017; 214: 2387–2404.
- McQuattie-Pimentel AC, Ren Z, Joshi N, *et al.* The aging microenvironment shapes alveolar macrophage identity in aging. *bioRxiv* 2019; preprint [https://doi.org/10.1101/717033].
- Gibbings SL, Thomas SM, Atif SM, *et al.* Three unique interstitial macrophages in the murine lung at steady state. *Am J Respir Cell Mol Biol* 2017; 57: 66–76.
- Loyher PL, Hamon P, Laviron M, *et al.* Macrophages of distinct origins contribute to tumor development in the lung. *J Exp Med* 2018; 215: 2536–2553.
- Lim HY, Lim SY, Tan CK, *et al.* Hyaluronan receptor LYVE-1-expressing macrophages maintain arterial tone through hyaluronan-mediated regulation of smooth muscle cell collagen. *Immunity* 2018; 49: 326–341.
- Chakarov S, Lim HY, Tan L, *et al.* Two distinct interstitial macrophage populations coexist across tissues in specific subtissular niches. *Science* 2019; 363: eaau0964.
- Lavin Y, Winter D, Blecher-Gonen R, *et al.* Tissue-resident macrophage enhancer landscapes are shaped by the local microenvironment. *Cell* 2014; 159: 1312–1326.
- Gibbings SL, Goyal R, Desch AN, *et al.* Transcriptome analysis highlights the conserved difference between embryonic and postnatal-derived alveolar macrophages. *Blood* 2015; 126: 1357–1366.
- Dostert C, Petrilli V, Van Bruggen R, *et al.* Innate immune activation through Nalp3 inflammasome sensing of asbestos and silica. *Science* 2008; 320: 674–677.
- dos Santos G, Rogel MR, Baker MA, *et al.* Vimentin regulates activation of the NLRP3 inflammasome. *Nat Commun* 2015; 6: 6574.
- Yona S, Kim KW, Wolf Y, *et al.* Fate mapping reveals origins and dynamics of monocytes and tissue macrophages under homeostasis. *Immunity* 2013; 38: 79–91.
- Madisen L, Zwingman TA, Sunkin SM, *et al.* A robust and high-throughput Cre reporting and characterization system for the whole mouse brain. *Nat Neurosci* 2010; 13: 133–140.
- Cheresh P, Morales-Nebreda L, Kim SJ, *et al.* Asbestos-induced pulmonary fibrosis is augmented in 8-oxoguanine DNA glycosylase knockout mice. *Am J Respir Cell Mol Biol* 2015; 52: 25–36.
- Ruffell B, Chang-Strachan D, Chan V, *et al.* Macrophage IL-10 blocks CD8⁺ T cell-dependent responses to chemotherapy by suppressing IL-12 expression in intratumoral dendritic cells. *Cancer Cell* 2014; 26: 623–637.
- Stafford JH, Hirai T, Deng L, *et al.* Colony stimulating factor 1 receptor inhibition delays recurrence of glioblastoma after radiation by altering myeloid cell recruitment and polarization. *Neuro-oncology* 2016; 18: 797–806.
- Butler A, Hoffman P, Smibert P, *et al.* Integrating single-cell transcriptomic data across different conditions, technologies, and species. *Nat Biotechnol* 2018; 36: 411–420.
- Xie T, Wang Y, Deng N, *et al.* Single-cell deconvolution of fibroblast heterogeneity in mouse pulmonary fibrosis. *Cell Rep* 2018; 22: 3625–3640.
- Stuart T, Butler A, Hoffman P, *et al.* Comprehensive integration of single-cell data. *Cell* 2019; 177: 1888–1902.
- Hafemeister C, Satija R. Normalization and variance stabilization of single-cell RNA sequencing data using regularized negative binomial regression. *bioRxiv* 2019; preprint [https://doi.org/10.1101/576827].
- Ramilowski JA, Goldberg T, Harshbarger J, *et al.* A draft network of ligand-receptor-mediated multicellular signalling in human. *Nat Commun* 2015; 6: 7866.
- La Manno G, Soldatov R, Zeisel A, *et al.* RNA velocity of single cells. *Nature* 2018; 560: 494–498.
- Kamp DW, Israbian VA, Yeldandi AV, *et al.* Phytic acid, an iron chelator, attenuates pulmonary inflammation and fibrosis in rats after intratracheal instillation of asbestos. *Toxicol Pathol* 1995; 23: 689–695.
- Davis AP, Grondin CJ, Johnson RJ, *et al.* The Comparative Toxicogenomics Database: update 2017. *Nucleic Acids Res* 2017; 45: D972–D978.

- 32 Gautier EL, Shay T, Miller J, *et al.* Gene-expression profiles and transcriptional regulatory pathways that underlie the identity and diversity of mouse tissue macrophages. *Nat Immunol* 2012; 13: 1118–1128.
- 33 Whitsett JA, Alenghat T. Respiratory epithelial cells orchestrate pulmonary innate immunity. *Nat Immunol* 2015; 16: 27–35.
- 34 Sauter KA, Pridans C, Sehgal A, *et al.* Pleiotropic effects of extended blockade of CSF1R signaling in adult mice. *J Leukoc Biol* 2014; 96: 265–274.
- 35 Shibata Y, Zsengeller Z, Otake K, *et al.* Alveolar macrophage deficiency in osteopetrotic mice deficient in macrophage colony-stimulating factor is spontaneously corrected with age and associated with matrix metalloproteinase expression and emphysema. *Blood* 2001; 98: 2845–2852.
- 36 Witmer-Pack MD, Hughes DA, Schuler G, *et al.* Identification of macrophages and dendritic cells in the osteopetrotic (op/op) mouse. *J Cell Sci* 1993; 104: 1021–1029.
- 37 Strunz M, Simon LM, Ansari M, *et al.* Longitudinal single cell transcriptomics reveals Krt8+ alveolar epithelial progenitors in lung regeneration. *bioRxiv* 2019; preprint [https://doi.org/10.1101/705244].
- 38 Liu T, Yu H, Ullenbruch M, *et al.* The *in vivo* fibrotic role of FIZZ1 in pulmonary fibrosis. *PLoS One* 2014; 9: e88362.
- 39 Lotfollahi M, Wolf FA, Theis FJ. scGen predicts single-cell perturbation responses. *Nat Methods* 2019; 16: 715–721.
- 40 Guilliams M, Scott CL. Does niche competition determine the origin of tissue-resident macrophages? *Nat Rev Immunol* 2017; 17: 451–460.
- 41 Zhou X, Franklin RA, Adler M, *et al.* Circuit design features of a stable two-cell system. *Cell* 2018; 172: 744–757.
- 42 Morse C, Tabib T, Sembrat J, *et al.* Proliferating SPP1/MERTK-expressing macrophages in idiopathic pulmonary fibrosis. *Eur Respir J* 2019; 54: 1802441.
- 43 Adler M, Mayo A, Zhou X, *et al.* Principles of cell circuits for tissue repair and fibrosis. *bioRxiv* 2019; preprint [https://doi.org/10.1101/710012].
- 44 Herrera J, Forster C, Pengo T, *et al.* Registration of the extracellular matrix components constituting the fibroblastic focus in idiopathic pulmonary fibrosis. *JCI Insight* 2019; 4: 125185.
- 45 Martinet Y, Rom WN, Grotendorst GR, *et al.* Exaggerated spontaneous release of platelet-derived growth factor by alveolar macrophages from patients with idiopathic pulmonary fibrosis. *N Engl J Med* 1987; 317: 202–209.
- 46 Nagaoka I, Trapnell BC, Crystal RG. Upregulation of platelet-derived growth factor-A and -B gene expression in alveolar macrophages of individuals with idiopathic pulmonary fibrosis. *J Clin Invest* 1990; 85: 2023–2027.
- 47 Meziani L, Mondini M, Petit B, *et al.* CSF1R inhibition prevents radiation pulmonary fibrosis by depletion of interstitial macrophages. *Eur Respir J* 2018; 51: 1702120.
- 48 McCubbrey AL, Barthel L, Mohning MP, *et al.* Deletion of c-FLIP from CD11b^{hi} macrophages prevents development of bleomycin-induced lung fibrosis. *Am J Respir Cell Mol Biol* 2018; 58: 66–78.
- 49 Aran D, Looney AP, Liu L, *et al.* Reference-based analysis of lung single-cell sequencing reveals a transitional profibrotic macrophage. *Nat Immunol* 2019; 20: 163–172.
- 50 Yu X, Buttgerit A, Lelios I, *et al.* The cytokine TGF-beta promotes the development and homeostasis of alveolar macrophages. *Immunity* 2017; 47: 903–912.
- 51 Sinclair C, Bommakanti G, Gardinassi L, *et al.* mTOR regulates metabolic adaptation of APCs in the lung and controls the outcome of allergic inflammation. *Science* 2017; 357: 1014–1021.
- 52 Schneider C, Nobs SP, Kurrer M, *et al.* Induction of the nuclear receptor PPAR-gamma by the cytokine GM-CSF is critical for the differentiation of fetal monocytes into alveolar macrophages. *Nat Immunol* 2014; 15: 1026–1037.
- 53 Zepp JA, Zacharias WJ, Frank DB, *et al.* Distinct mesenchymal lineages and niches promote epithelial self-renewal and myofibrogenesis in the lung. *Cell* 2017; 170: 1134–1148.
- 54 Wu H, Kiritani Y, Donnelly EL, *et al.* Advantages of single-nucleus over single-cell RNA sequencing of adult kidney: rare cell types and novel cell states revealed in fibrosis. *J Am Soc Nephrol* 2019; 30: 23–32.